

DIFFUSE Ly α EMITTING HALOS: A GENERIC PROPERTY OF HIGH-REDSHIFT STAR-FORMING GALAXIES*

CHARLES C. STEIDEL¹, MILAN BOGOSAVLJEVIĆ^{1,2}, ALICE E. SHAPLEY^{3,9,10}, JUNA A. KOLLMEIER⁴,
 NAVEEN A. REDDY^{5,11}, DAWN K. ERB^{6,7,12}, AND MAX PETTINI⁸

¹ California Institute of Technology, MS 249-17, Pasadena, CA 91125, USA

² Astronomical Observatory, Volgina 7, 11060 Belgrade, Serbia

³ Department of Physics and Astronomy, University of California, Los Angeles, 430 Portola Plaza, Box 951547, Los Angeles, CA 90095, USA

⁴ Carnegie Observatories, 813 Santa Barbara Street, Pasadena, CA 91101, USA

⁵ National Optical Astronomy Observatories, 950 North Cherry Avenue, Tucson, AZ 85258, USA

⁶ Department of Physics, University of California Santa Barbara, Santa Barbara, CA 93106, USA

⁷ Department of Physics, University of Wisconsin-Milwaukee, P.O. Box 413, Milwaukee, WI 53201, USA

⁸ Institute of Astronomy, Madingley Road, Cambridge CB3 0HA, UK

Received 2011 January 10; accepted 2011 May 24; published 2011 July 19

ABSTRACT

Using a sample of 92 UV continuum-selected, spectroscopically identified galaxies with $\langle z \rangle = 2.65$, all of which have been imaged in the Ly α line with extremely deep narrow-band imaging, we examine galaxy Ly α emission profiles to very faint surface brightness limits. The galaxy sample is representative of spectroscopic samples of Lyman break galaxies (LBGs) at similar redshifts in terms of apparent magnitude, UV luminosity, inferred extinction, and star formation rate and was assembled without regard to Ly α emission properties. Approximately 45% (55%) of the galaxy spectra have Ly α appearing in net absorption (emission), with $\simeq 20\%$ satisfying commonly used criteria for the identification of “Ly α emitters” (LAEs; $W_0(\text{Ly}\alpha) \geq 20 \text{ \AA}$). We use extremely deep stacks of rest-UV continuum and continuum-subtracted Ly α images to show that all sub-samples exhibit diffuse Ly α emission to radii of at least $10''$ (~ 80 physical kpc). The characteristic exponential scale lengths for Ly α line emission exceed that of the $\lambda_0 = 1220 \text{ \AA}$ UV continuum light by factors of ~ 5 – 10 . The surface brightness profiles of Ly α emission are strongly suppressed relative to the UV continuum light in the inner few kpc, by amounts that are tightly correlated with the galaxies’ observed spectral morphology; however, all galaxy sub-samples, including that of galaxies for which Ly α appears in net absorption in the spectra, exhibit qualitatively similar diffuse Ly α emission halos. Accounting for the extended Ly α emission halos, which generally would not be detected in the slit spectra of individual objects or with typical narrow-band Ly α imaging, increases the total Ly α flux (and rest equivalent width $W_0(\text{Ly}\alpha)$) by an average factor of ~ 5 , and by a much larger factor for the 80% of LBGs not classified as LAEs. We argue that most, if not all, of the observed Ly α emission in the diffuse halos originates in the galaxy H II regions but is scattered in our direction by H I gas in the galaxy’s circum-galactic medium. The overall intensity of Ly α halos, but not the surface brightness distribution, is strongly correlated with the emission observed in the central $\sim 1''$ —more luminous halos are observed for galaxies with stronger central Ly α emission. We show that whether or not a galaxy is classified as a giant “Ly α blob” (LAB) depends sensitively on the Ly α surface brightness threshold reached by an observation. Accounting for diffuse Ly α halos, all LBGs would be LABs if surveys were sensitive to 10 times lower Ly α surface brightness thresholds; similarly, essentially all LBGs would qualify as LAEs.

Key words: cosmology: observations – galaxies: evolution – galaxies: high-redshift

Online-only material: color figures

1. INTRODUCTION

Although the Ly α emission line of neutral H is expected to be produced in prodigious amounts by star-forming galaxies (e.g., Partridge & Peebles 1967; Meier 1976), it has long been appreciated that the astrophysics affecting observations of Ly α are far more complex than for other lines of abundant species due to resonant scattering (Spitzer 1978; Meier & Terlevich 1981; Charlott & Fall 1993). The very large cross section in the Ly α transition means that emission from a gas cloud or nebula may have been strongly altered in intensity, kinematics, and apparent

spatial distribution by the time it reaches an observer. Similarly, information about the initial source of observed Ly α emission may be lost or obscured, with the apparent source simply being H I gas responsible for scattering in the observer’s direction. Consequently, the dominant process producing Ly α emission may often be ambiguous; possibilities include photoionization by young stars or active galactic nuclei, line emission following collisional excitation of H atoms, or simply scattering from intervening H I gas that happens to favor the observer’s direction.

In the absence of dust, the standard expectation for Ly α emission produced in H II regions for “Case B” (i.e., ionization-bounded) recombination (Brocklehurst 1971) and a Chabrier (2003) stellar initial mass function (IMF) for high-mass stars¹³ is that each solar mass of star formation produces an Ly α luminosity $L(\text{Ly}\alpha) \simeq 2.0 \times 10^{42} \text{ erg s}^{-1}$. For the same IMF,

* Based on data obtained at the W. M. Keck Observatory, which is operated as a scientific partnership among the California Institute of Technology, the University of California, and NASA, and was made possible by the generous financial support of the W. M. Keck Foundation.

⁹ Alfred P. Sloan Fellow.

¹⁰ Packard Fellow.

¹¹ Hubble Fellow.

¹² Spitzer Fellow.

¹³ Note that this value is a factor 1.8 higher than would be obtained assuming a Salpeter (1955) IMF because a given number of ionizing photons is associated with a smaller total SFR for the Chabrier IMF.

the far-UV continuum light produced per solar mass of star formation rate (SFR) near the wavelength of Ly α has an expected monochromatic luminosity in the range $40.0 \text{ erg s}^{-1} \text{ \AA}^{-1} \lesssim \log L_{\lambda, \text{cont}} \lesssim 40.3 \text{ erg s}^{-1} \text{ \AA}^{-1}$ (Leitherer et al. 1999). The predicted rest equivalent width of Ly α emission is then given by $W_0(\text{Ly}\alpha) \simeq L(\text{Ly}\alpha)/L_{\lambda, \text{cont}} \simeq 100\text{--}200 \text{ \AA}$ (see also Charlot & Fall 1993), with values near the lower end of this range expected for continuous star formation lasting more than $\sim 3 \times 10^7 \text{ yr}$, roughly the minimum dynamical timescale for L^* Lyman break galaxies (LBGs) at $z \sim 2\text{--}3$ (e.g., Erb et al. 2006b). Under the above assumptions, the period of time over which Ly α emission has $W_0(\text{Ly}\alpha) > 100 \text{ \AA}$ would be very brief, after which the line-to-continuum ratio reaches an asymptotic value of $W_0(\text{Ly}\alpha) \simeq 100 \text{ \AA}$. Thus, for a UV continuum-selected sample, one would expect very few galaxies to be caught during a time when their intrinsic $W_0(\text{Ly}\alpha)$ exceeds 100 \AA .¹⁴

When dust is mixed throughout the scattering medium, one expects selective extinction of Ly α photons compared to those in the nearby UV continuum due to the much larger effective path length traversed by a line photon before escaping into the intergalactic medium (e.g., Meier & Terlevich 1981; Hartmann et al. 1984; Neufeld 1990). This effect is often cited when observed Ly α emission lines are much weaker than the Case B expectations discussed above (e.g., Charlot & Fall 1993; Shapley et al. 2003; Hayes et al. 2010; Kornei et al. 2010). Since most continuum-selected high-redshift galaxies in current spectroscopic surveys appear to have at least some dust, and the vast majority have Ly α equivalent widths $W_0(\text{Ly}\alpha) < 100 \text{ \AA}$ (e.g., Shapley et al. 2003; Kornei et al. 2010), this conclusion would seem reasonable. On the other hand, it is also possible, at least in principle, for Ly α photons to experience *less* attenuation by dust than continuum photons, in the case of a clumpy interstellar medium (ISM) in which dust is located only within the clumps, which are rarely penetrated by Ly α photons (Neufeld 1991; Finkelstein et al. 2008). There is no reason to believe that the two competing effects could not *both* be at work within different regions of the same galaxy.

Even without dust, however, resonant scattering produces spatial and/or spectral diffusion of Ly α photons leading to emergent line emission whose properties depend on the geometry, kinematics, and H I optical depth distributions within the gaseous circum-galactic medium (CGM) surrounding a galaxy (Steidel et al. 2010, hereafter S2010). In the zero-dust case, the total Ly α luminosity would be unaltered by resonant scattering, but, as we detail below, the *detectability* of Ly α could be very strongly affected.

In S2010, we characterized the distribution of cool gas in the CGM of star-forming galaxies with redshifts $2 \lesssim z \lesssim 3$ and attempted to understand the kinematics and line strength of the ISM absorption and Ly α emission in the context of galaxy-scale gaseous outflows. In brief, we found that UV-selected galaxies within a factor of a few of L^* in the far-UV continuum luminosity function (corresponding at $z \sim 2.5$ to apparent magnitudes $\mathcal{R} \simeq 24\text{--}24.5$ —see Reddy & Steidel 2009) have a CGM that can be traced by H I (Ly α and Ly β absorption) and several strong absorption lines of metallic species (e.g., C II, C IV, Si II, Si IV) to galactocentric distances of $\lesssim 120 \text{ kpc}$ using the spectra of faint background galaxies. The measurement used more than 500 galaxy pairs on angular scales $1''\text{--}15''$ to map out the absorption line strength as a function of galaxy

impact parameter b (i.e., the physical separation of the two lines of sight at the redshift of the foreground galaxy) for each observed species. In slit spectra of the CGM “host galaxies,” the bulk of observed Ly α emission, when present, is almost always strongly redshifted, while the strong interstellar (IS) absorption lines are strongly blueshifted. S2010 presented a geometric and kinematic model that reproduces many of the observed trends. In the model, Ly α photons escape the galaxy in an observer’s direction mainly by scattering from optically thick H I gas located on the far side of the galaxy’s stars, but having the same overall (outflowing) kinematics as the IS gas seen in blueshifted absorption. We used the transverse information from the galaxy pairs combined with line-of-sight information available from the galaxies’ own far-UV spectra to construct a consistent geometric and kinematic model of galaxy-scale outflows in the context of a very well-studied population of high-redshift star-forming galaxies. That is, we combined the line profiles of IS absorption lines and Ly α emission in the galaxy spectra themselves (sampling the kinematics and line strength for galactocentric impact parameter $b \sim 0$) with IS line strength measurements at $b \gg 0$ (using close angular pairs of galaxies) to infer the three-dimensional distribution of CGM gas surrounding an average galaxy in the spectroscopic sample. We suggested that the CGM gas seen in absorption would also constitute a scattering medium through which Ly α photons must traverse in order to be observed. High velocities and large velocity gradients together with gas covering fraction $f_c \leq 1$ through much of the CGM allow Ly α photons to diffuse spatially outward, favoring escape of Ly α photons last scattered (in the observer’s direction) from atoms with velocities well off resonance with respect to any H I that remains between the location of the last scattering and the observer. If true, one might then expect to observe scattered Ly α emission over the same spatial scales for which strong H I and low-ion metallic absorption is seen, i.e., $\simeq 80\text{--}90 \text{ kpc}$, even if all Ly α photons originated in the galaxy’s H II regions.

Clearly, scattering will substantially modify both the spatial and spectral distribution of Ly α photons emergent in a particular direction, and at the very least may cause Ly α emitting regions to appear distinct from the UV continuum emission even if both share a common origin. Slit spectra commonly optimized for the compact size of the continuum emitting regions of typical star-forming high-redshift galaxies may encompass only a fraction of emergent Ly α emission. The relevant angular scale for the optically thick CGM H I gas is $\simeq 10''$ ($\simeq 80 \text{ physical kpc}$ at $z \sim 2.5$), whereas a typical extraction aperture for a slit spectrum is $\sim 1''.2 \times 1''.4$ —a difference of a factor of more than 180 in solid angle. Thus, even if the Case B expected production rate of Ly α photons were to escape the CGM of a galaxy, it is likely that the emission would be distributed over such a large region that a narrow slit would miss most of the Ly α flux; even very deep narrow-band (NB) images might leave much of the flux unaccounted for due to limited surface brightness sensitivity.

In this paper, we present direct observational evidence showing that extended Ly α scattering “halos” are a generic property of high-redshift star-forming galaxies, including those that have no apparent Ly α emission lines in their far-UV spectra. In Section 2, we describe a sample of 92 UV-continuum-selected galaxies for which both rest-far-UV spectra and deep NB Ly α images are available, and discuss the relationship between Ly α properties measured using both techniques. In Section 3, we use composite UV spectra, as well as Ly α and continuum image stacking, to measure Ly α emission extending to very low sur-

¹⁴ For a sample selected by Ly α (as opposed to continuum) emission, this may not be the case.

Table 1
Summary of Ly α Narrow-band Observations

Field	NB Filter ^a	z Range ^b	Number ^c	Telescope/Instrument	Date	t_{exp} ^d	PSF ^e	$S(\text{Ly}\alpha, \text{obs})^f$	$S(\text{Ly}\alpha, z = 2.65)^g$
HS1549+195	4667/88	2.802–2.875	27	Keck 1 10 m/LRIS	2007 Mar/2010 May	18000	0''.86	1.29	1.59
HS1700+643	4018/90	2.266–2.340	43	Palomar 5 m/LFC	2007 Jul	80280	1''.20	2.30	1.54
SSA22a ^h	4980/80	3.063–3.129	22	Keck 1 10 m/LRIS	2005 Aug	33880	0''.80	0.94	1.50
				Subaru 8 m/SuprimeCam	2002 Sep	25800			

Notes.

^a Central wavelength/bandwidth of NB filter, in Å.

^b Redshift range included between NB filter half-power points.

^c Number of continuum-selected, spectroscopically identified galaxies with NB measurements.

^d Total integration time, in seconds.

^e Stellar FWHM in arcseconds after smoothing to match the CB and NB PSF prior to photometry.

^f Observed surface brightness isophotal threshold (1.5σ), in units of $10^{-18} \text{ erg s}^{-1} \text{ cm}^{-2} \text{ arcsec}^{-2}$.

^g Isophotal surface brightness threshold, corrected to $z = 2.65$, in units of $10^{-18} \text{ erg s}^{-1} \text{ cm}^{-2} \text{ arcsec}^{-2}$.

^h The field imaged with Keck/LRIS is a $5'.5 \times 7'.6$ subset of the LBG survey field from Steidel et al. (2003, 2000). The NB image is a combination of the LRIS images and archival Subaru images, discussed by Nestor et al. (2011).

face brightness thresholds for various galaxy sub-samples. The results and their implications for the nature of Ly α emission in star-forming galaxies are described in Section 4, discussed in Section 5, and summarized in Section 6.

Throughout the paper, we assume a Λ CDM cosmology with $\Omega_m = 0.3$, $\Omega_\Lambda = 0.7$, and $h = 0.7$.

2. THE GALAXY SAMPLE

The galaxies used in this paper are drawn from three survey regions where we used UV-color selection to select galaxies with $1.8 \lesssim z \lesssim 3.4$ for spectroscopy (Steidel et al. 2003, 2004; Shapley et al. 2005). In addition to completing extensive LBG spectroscopic follow-up, we have also imaged the three regions using NB filters centered at the observed wavelength of Ly α at the redshift of galaxy overdensities we had previously identified from the continuum-selected spectroscopic sample. Table 1 summarizes the NB observations in these fields, all of which are among the deepest NB images ever obtained for Ly α at redshifts $z \sim 2$ –3. The number of continuum-selected galaxies with spectroscopic redshifts falling within the redshift range subtended by the NB filter bandpass in each field are also summarized in Table 1.

We now briefly comment on each of the fields observed.

1. SSA22a has a redshift “spike” centered at $z = 3.09$ (Steidel et al. 1998, 2003) which was first identified from the spectroscopic follow-up of LBGs. It was first imaged in Ly α at the same redshift by Steidel et al. (2000), who discovered two very large (> 100 kpc) “Ly α blobs” (LABs), prompting several subsequent studies of Ly α -selected objects using deeper NB data (e.g., Matsuda et al. 2004; Hayashino et al. 2004; Nestor et al. 2011). Here we include the 22 continuum color-selected LBGs with spectroscopic redshifts (Steidel et al. 2003; Shapley et al. 2006) lying within a $5'.5 \times 7'.6$ region with especially deep Ly α NB observations (Table 1).
2. HS1700+64 is a survey field centered on the position of a hyper-luminous ($r' = 16.0$, or $L \simeq 1.1 \times 10^{14} L_\odot$) $z = 2.751$ quasi-stellar object (QSO). A galaxy overdensity was again identified from spectroscopic follow-up, with $z = 2.299 \pm 0.03$ (Shapley et al. 2005; Steidel et al. 2005). We have subsequently obtained very deep NB imaging in both H α and Ly α at this redshift (D. K. Erb et al. 2011, in preparation). We include in the present sample the 43 continuum-selected galaxies with spectroscopic redshifts

placing the Ly α transition within an NB filter designed for follow-up of the protocluster.

3. HS1549+195 is another survey field centered on the position of a hyper-luminous QSO ($r' = 15.9$, or $L \simeq 1.4 \times 10^{14} L_\odot$), with $z_Q = 2.842$. Once again a galaxy overdensity was identified from the LBG spectroscopic follow-up, in this case centered on the redshift of the QSO itself.¹⁵ The NB4670 filter was designed to follow up on the galaxy overdensity, and in response to the serendipitous discovery of spatially offset (and plausibly fluorescent) Ly α emission associated with a $z = 2.842$ damped Ly α absorption system identified in the spectrum of a faint background QSO (Adelberger et al. 2006).

In all three fields used in the present paper, galaxies were selected using rest-UV (LBG) color selection and observed spectroscopically using the Keck 1 10 m telescope and LRIS spectrograph (Oke et al. 1995; Steidel et al. 2004) prior to the Ly α imaging, so the resulting sample should be relatively unbiased with respect to Ly α properties. The full sample of 92 galaxies with mean redshift $\langle z \rangle = 2.65$ is broadly representative of UV-selected spectroscopic samples (e.g., Steidel et al. 2003, 2004; Shapley et al. 2003; Adelberger et al. 2004) in terms of both continuum and Ly α properties: for example, they have $23.4 \leq \mathcal{R}_{\text{AB}} \leq 25.5$ with median (mean) of $\mathcal{R}_{\text{AB}} = 24.47$ (24.50), and spectroscopically measured $W_0(\text{Ly}\alpha)$ in the range -37 \AA (absorption) to $+89 \text{ \AA}$ (emission) with median $W_0(\text{Ly}\alpha) \simeq +0.9 \text{ \AA}$ (cf. Shapley et al. 2003; Reddy et al. 2008; Kornei et al. 2010). The spectroscopic measures of Ly α are based on extraction apertures of angular size $1''.2$ (the slit width) by $\simeq 1''.35$, independent of wavelength, so that Ly α and the UV continuum light are measured over identical spatial regions. We used a method similar to that described by Kornei et al. (2010) to measure $W_0(\text{Ly}\alpha)$ directly from the galaxy spectra.

Ly α equivalent widths (and fluxes) were also measured for the same set of 92 galaxies using a comparison of deep NB and continuum (CB) images. As discussed by, e.g., Steidel et al. (2000), care must be taken since spectroscopic and imaging measurements of Ly α may not be measuring the same quantities. For measurements of Ly α line emission from CB – NB color, the photometric aperture is often defined by the region within an

¹⁵ As we will show below, there is no evidence that the presence of the QSO has significantly altered the overall Ly α emission of the galaxies at the same redshift.

isophote corresponding to a particular Ly α surface brightness threshold, which of course depends on the depth of the Ly α image. It also depends on the suitability of the continuum measurement for estimating the UV continuum flux density in the vicinity of the Ly α line, which may require a color-term correction and/or correction for Ly α line contamination. The three Ly α images used here are comparably deep to the deepest Ly α surveys to date, with 1σ surface brightness thresholds of $1.53, 0.86,$ and $0.63 \times 10^{-18} \text{ erg s}^{-1} \text{ cm}^{-2} \text{ arcsec}^{-2}$ for the HS1700, HS1549, and SSA22 fields, respectively.¹⁶ Although these observed surface brightness (SB) thresholds differ by a factor of more than two, the deeper data at higher redshift result in rest-frame Ly α surface brightness thresholds which differ by less than 10%. The last column of Table 1 shows the relative surface brightness thresholds when all three data sets are shifted to the mean redshift of $\langle z \rangle = 2.65$.

Important to generating Ly α line images for relatively continuum-bright galaxies (and for measuring line equivalent widths independently of spectroscopy) is a measure of their far-UV continuum (hereinafter CB, or $m_{\text{AB}}[1220 \text{ \AA}]$) near the wavelength of the Ly α line. Ideally, the CB should have the same effective wavelength as the NB without including the Ly α line itself. For the three fields presented here, deep CB images were created using linear combinations of two broadband filters bracketing the NB passband; details of these procedures are described in the individual papers cited above. Briefly, in HS1700 we used very deep $U_n(3550/700)$ and $G(4730/1100)$ images obtained in 2001 May with the William Herschel 4.2 m Telescope prime focus imager (see Shapley et al. 2005) to create a “UG” continuum image with an effective wavelength of 4010 \AA . For SSA22a, we used archival B and V images taken with the 8.2 m Subaru telescope with SuprimeCam to create a “BV” CB image with $\lambda_{\text{eff}} = 4980 \text{ \AA}$ (see Nestor et al. 2011). The HS1549 field was treated somewhat differently, since the deepest broadband image (10,800 s integration with Keck/LRIS) was obtained in the V band¹⁷ using the LRIS red channel contemporaneously with the 2007 March NB4670 images on the blue channel. A less-deep G -band image (2500 s with Keck/LRIS-B) was used to estimate the appropriate (object-dependent) color correction needed to adjust the deeper V -band images to an effective wavelength near 4670 \AA . Since the observed range in continuum color among the sample galaxies at a given redshift is small (e.g., the mean and standard deviation in observed broadband color for the 43 $z \simeq 2.30$ galaxies in the HS1700 field is $\langle G - R \rangle = 0.26 \pm 0.12$, and $\langle U_n - G \rangle = 0.80 \pm 0.20$ where the errors include photometric scatter), and the passbands are separated by only $\simeq 300 \text{ \AA}$ in the galaxy rest frame, we believe that systematic errors associated with producing the CB image at the appropriate effective wavelength is likely very small ($\ll 0.1 \text{ mag}$).

In brief, the CB and NB images were first scaled to have matching zero points based on photometry of spectrophotometric standard stars and by calculating the relative system throughput in each filter passband as a cross-check. The suitably scaled CB or NB images were smoothed using a Gaussian kernel to match the stellar point-spread functions (PSFs) in the two images; the final PSF size for each field is listed in Table 1. Matched aperture photometry was performed using dual image mode in

SExtractor (Bertin & Arnouts 1996), with CB – NB colors measured using photometric apertures defined in the NB image at an isophotal threshold equivalent to 1.5σ per pixel above the estimated local sky background. The CB zero point was iteratively adjusted by a small amount ($< 0.1 \text{ mag}$ in all cases) so that the median color of all objects in the image having $23 \leq \text{CB} \leq 26$ (the principle range expected for the galaxies of interest) has CB – NB = 0, corresponding to identical flux density measured in each band. The statistical error in the measurement of CB – NB can be conservatively estimated from the dispersion in color for all objects in the same range of apparent magnitude, which is quite small because of the intrinsically narrow range in color and the depth of both the CB and NB images ($\sigma(\text{CB} - \text{NB}) \simeq 0.05\text{--}0.1 \text{ mag}$). A continuum-subtracted Ly α line image (hereinafter “Ly α ” image) was formed by subtracting the scaled continuum image from the NB image.¹⁸

We measured $W(\text{Ly}\alpha)$ (in units of \AA) from the CB – NB color using the simple relationship

$$W_0(\text{Ly}\alpha) = B_{\text{NB}} [10^{0.4|\text{CB}-\text{NB}|} - 1] \frac{\text{CB} - \text{NB}}{|\text{CB} - \text{NB}|} \text{\AA}, \quad (1)$$

where B_{NB} is the appropriate rest-frame bandwidth in \AA of the NB filter (19.6 \AA , 23.4 \AA , and 27.3 \AA for SSA22, HS1549, and HS1700, respectively). Note that with this definition, $W_0(\text{Ly}\alpha) = 0$ when CB = NB, and positive (negative) values indicate net Ly α emission (absorption). At an isophotal threshold of $\simeq 1.5 \times 10^{-18} \text{ erg s}^{-1} \text{ cm}^{-2} \text{ arcsec}^{-2}$, the typical solid angle subtended by the detection isophote in the NB image for the continuum-selected galaxies is $\simeq 3.8 \text{ arcsec}^2$, ~ 2.3 times larger than the spectroscopic aperture. If the spatial distribution of Ly α emission is significantly different from that of the continuum light, then the measured colors (and hence the inferred $W_0(\text{Ly}\alpha)$) could differ from the spectroscopic values. Figure 1 compares the measurements of $W_0(\text{Ly}\alpha)$ from the spectra versus those based on the CB – NB colors for the same 92 galaxies in the current sample, while Figure 2 compares the two distributions. There is a modest tendency for the value of $W_0(\text{Ly}\alpha)$ measured from the NB images to be larger in absolute value (whether in absorption or emission) near the extremes of the distribution, though they have very similar mean and median values (Figure 2) and agree well when $|W_0|$ is small. If significant Ly α flux were distributed on still larger angular scales (with lower Ly α surface brightness) while the same is not true of the UV continuum light, then even the larger NB-based $W_0(\text{Ly}\alpha)$ would underestimate the true values.

3. INFERENCES FROM STACKED COMPOSITES

3.1. Spectroscopic Stacks

In order to measure Ly α emission with SB well below the detection threshold for individual objects, we constructed composite spectra and images after dividing the sample of 92 into several subsets, summarized in Table 2. We used the values of $W_0(\text{Ly}\alpha)$ measured from the CB – NB colors for all galaxies, with apertures defined by the isophotal thresholds listed in Column 9 of Table 1. This method has generally smaller statistical uncertainties and aperture corrections compared with the spectroscopic measurements, and facilitates comparison

¹⁶ Isophotal apertures corresponding to 1.5σ above the local sky were used for NB-selected catalogs in all three cases.

¹⁷ Because the data were obtained using a dichroic with a transition wavelength of $\simeq 5000 \text{ \AA}$ (d500), the V passband was shifted to slightly longer wavelength ($\lambda_{\text{eff}} \simeq 5506 \text{ \AA}$ instead of 5464 \AA).

¹⁸ Among the three fields, only the SSA22a CB includes a small overlap ($\simeq 2.5\%$ of its full bandwidth) with the NB Ly α passband; this would have the effect of a small (negligible for our purposes) oversubtraction of the continuum when producing the Ly α line image.

Table 2
Ly α and Continuum Surface Brightness Profiles for Composites

Sample ^a	Number	$\langle z \rangle$	$\langle m_{AB} \rangle^b$ (1220 Å)	C_l^c (10^{-18})	b_l^c (kpc)	C_c^c (10^{-18})	b_c^c (kpc)	$F(\text{Ly}\alpha)^d$ (10^{-16})	$L_{\text{tot}}(\text{Ly}\alpha)^e$ (10^{42} erg s $^{-1}$)	$W_0(\text{Ly}\alpha, \text{spec})^f$ (Å)	$W_0(\text{Ly}\alpha, \text{tot})^g$ (Å)
All	92	2.65	24.60	2.4	25.2	87.2	3.4	1.7	9.7	+6.9	+36.0
Ly α Em	52	2.66	24.40	3.1	25.6	136.3	2.9	2.5	14.3	+13.2	+44.9
Ly α Abs	40	2.63	24.72	1.5	20.8	52.5	4.5	0.7	4.0	−4.4	+16.8
All non-LAE	74	2.65	24.56	1.4	25.5	124.9	2.8	1.4	8.0	+1.0	+29.1
LAE only	18	2.64	24.68	3.9	28.4	110.3	2.9	4.0	22.8	+29.2	+92.9
Ly α blobs	11	2.59	...	15.7	27.6	11.5	65.7

Notes.

^a Galaxy sub-sample, drawn from the full sample (all) of 92 continuum-selected galaxies with Ly α imaging. The details of the sub-samples are described in the text.

^b Average continuum apparent magnitude at $\lambda_0 \simeq 1220$ Å, estimated from the CB photometry.

^c Best-fit parameters assuming SB profile $S(r) = C_n \exp(-b/b_n)$, where C_n is in units of 10^{-18} erg s $^{-1}$ cm $^{-2}$ arcsec $^{-2}$. The subscripts l and c refer to the Ly α line and UV continuum profiles, respectively.

^d Average integrated Ly α flux, in units of 10^{-16} erg s $^{-1}$ cm $^{-2}$.

^e Average integrated Ly α luminosity, in units of 10^{42} erg s $^{-1}$, assuming $\langle z \rangle = 2.65$.

^f Ly α rest equivalent width measured from spectrum (Figure 3).

^g Ly α rest equivalent width of total Ly α flux, in Å.

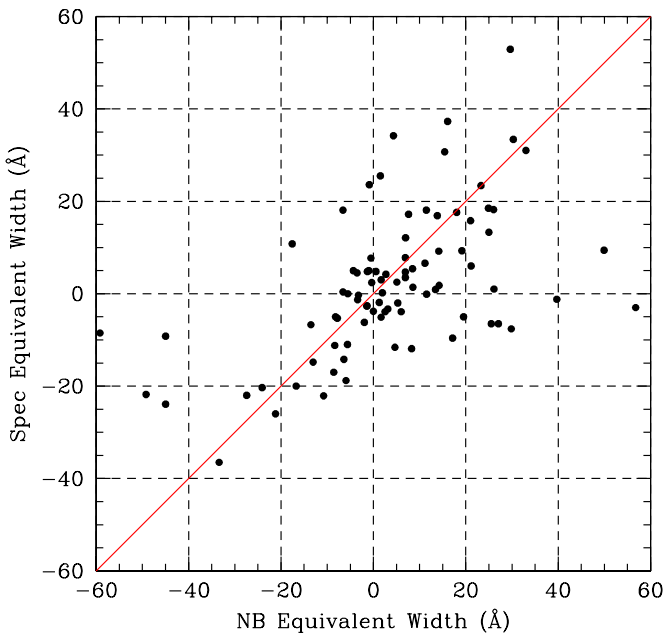


Figure 1. Comparison of Ly α line equivalent widths measured from spectra compared to those inferred from CB – NB colors in deep Ly α imaging. The imaging measurements use isophotal apertures defined by the extent of Ly α flux to a surface brightness limit of $\simeq(1-2) \times 10^{-18}$ erg s $^{-1}$ cm $^{-2}$ arcsec $^{-2}$, which is typical of the deepest Ly α narrow-band imaging surveys.

(A color version of this figure is available in the online journal.)

with most deep Ly α surveys, which are based primarily on equivalent widths and fluxes inferred from the NB photometry.¹⁹

As illustrated in Figure 2, the median $W_0(\text{Ly}\alpha)$ from both NB imaging and spectroscopic measurements is close to zero, in agreement with previous results for continuum-selected samples (Steidel et al. 2000; Shapley et al. 2003; Kornei et al. 2010). In forming subsets of the sample of 92, we used the NB Ly α measurements to split the sample into “Ly α Em,” those that have Ly α in net emission (52), and “Ly α Abs,” those having

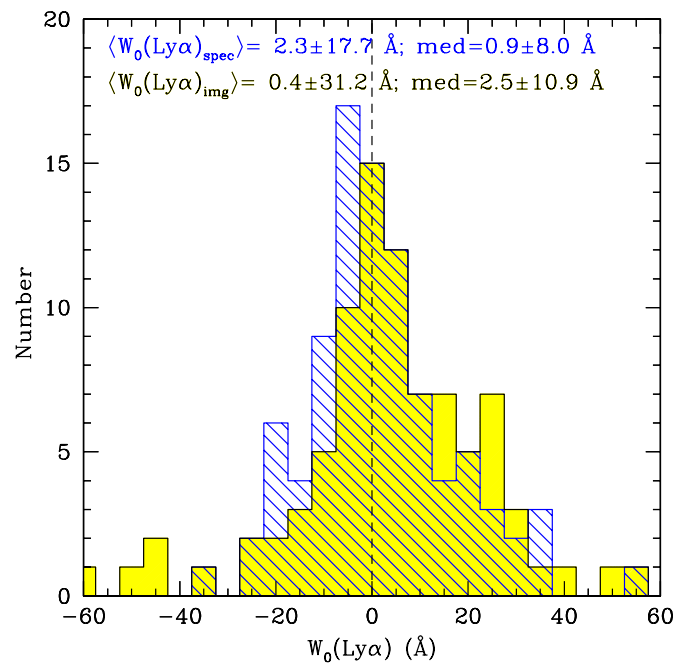


Figure 2. Comparison of the Ly α line equivalent width distribution from spectroscopic measurements vs. that inferred from CB – NB colors in Ly α imaging. The imaging measurements use colors within isophotal apertures defined by the extent of Ly α flux to a surface brightness limit of $\simeq(1-2) \times 10^{-18}$ erg s $^{-1}$ cm $^{-2}$ arcsec $^{-2}$, which is typical of the deepest Ly α narrow-band imaging surveys. The statistics are for the mean and standard deviation (left) of individual values (left), and the median and inter-quartile range (right) for each set of measurements.

(A color version of this figure is available in the online journal.)

Ly α in net absorption (40)—see the second and third rows of Table 2, respectively. Two other subsets were made consisting of galaxies satisfying the criteria commonly adopted for “Ly α emitters” (LAEs), i.e., $W_0(\text{Ly}\alpha) \geq 20$ Å, of which there are 18 (20% of the total), with the remainder (74 of 92, or 80%) placed in a sub-sample called “non-LAEs,” i.e., all continuum-selected LBGs that would not be selected as LAEs.

For each sub-sample listed in Table 2, a composite far-UV spectrum was created by shifting the observed, flux-calibrated

¹⁹ We have verified that none of the results of this paper depend significantly on whether the imaging or spectroscopic measures of Ly α are used to define the subsets.

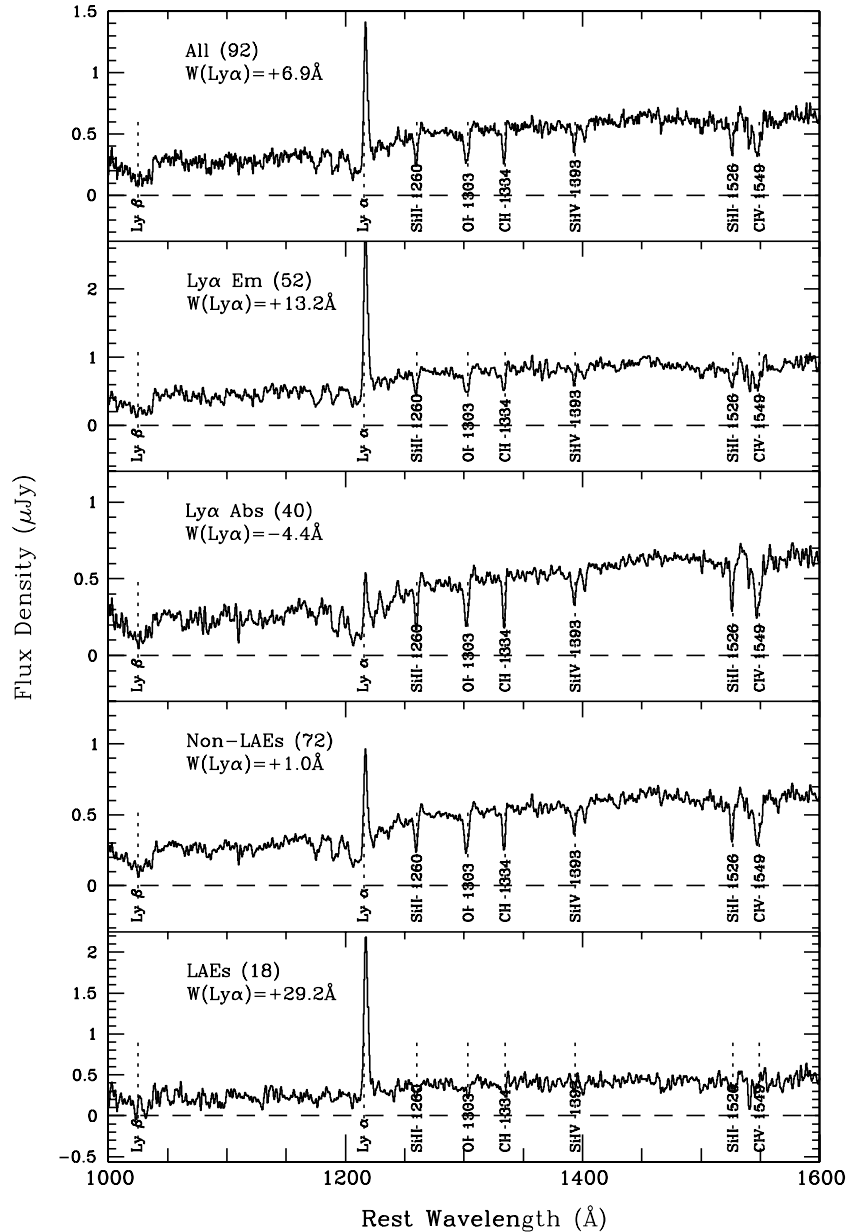


Figure 3. Composite spectra formed from the average within the sub-samples detailed in Table 2. Within each panel, the number of galaxies going into the stack is listed after the sub-sample name; the second line in the annotation lists the rest-frame equivalent width of the $\text{Ly}\alpha$ line measured from the composite spectrum, with the convention that positive values indicate net emission.

spectra into the galaxy rest frame using the prescriptions given in S2010, resampling the rest-frame spectra to 0.5 Å pixel^{-1} , and averaging. Each stacked composite spectrum was scaled so that the continuum level near $\text{Ly}\alpha$ matched that obtained from the photometric stack of the same subset of galaxies, discussed below. The correction was typically a factor of $\simeq 1.5$ and was applied for the sole purpose of placing the continuum levels for the same subsets on the same flux scale. The resulting stacked spectra are shown in Figure 3; measured properties of the composite spectra are given in the figure and listed in Table 2.

3.2. $\text{Ly}\alpha$ and CB Stacks

A $25'' \times 25''$ sub-image (“postage stamp”) centered on the position of the continuum centroid of each galaxy was extracted from the CB image and the (continuum-subtracted) $\text{Ly}\alpha$ images after scaling them to a common zero point as discussed above.

Masks were created by performing object detection on each continuum sub-image using SExtractor (Bertin & Arnouts 1996). These were used to exclude pixels lying within the detection isophotes of any object other than the central one, and were applied during the stacking to both the CB and $\text{Ly}\alpha$ images. Two stacked images were formed for each subset listed in Table 2 (straight averages, with masking), one for the CB image and another for the $\text{Ly}\alpha$ line image. Figure 4 compares the average CB image with the $\text{Ly}\alpha$ image for the full sample of 92 galaxies, while Figure 5 compares the azimuthally averaged surface brightness profiles of the same composite CB and $\text{Ly}\alpha$ images. Figure 4 shows clearly that, on average, $\text{Ly}\alpha$ emission is detected to radii of at least $10''$, or $\simeq 80$ physical kpc at $\langle z \rangle = 2.65$. Figure 5 shows that the average CB light profile for the same galaxies is much more compact and drops below the SB detection threshold for $b \gtrsim 20 \text{ kpc}$ ($\gtrsim 2''.5$). Figure 5 also shows what the $\text{Ly}\alpha$ line profile would look like if $W_0(\text{Ly}\alpha) = 100 \text{ Å}$

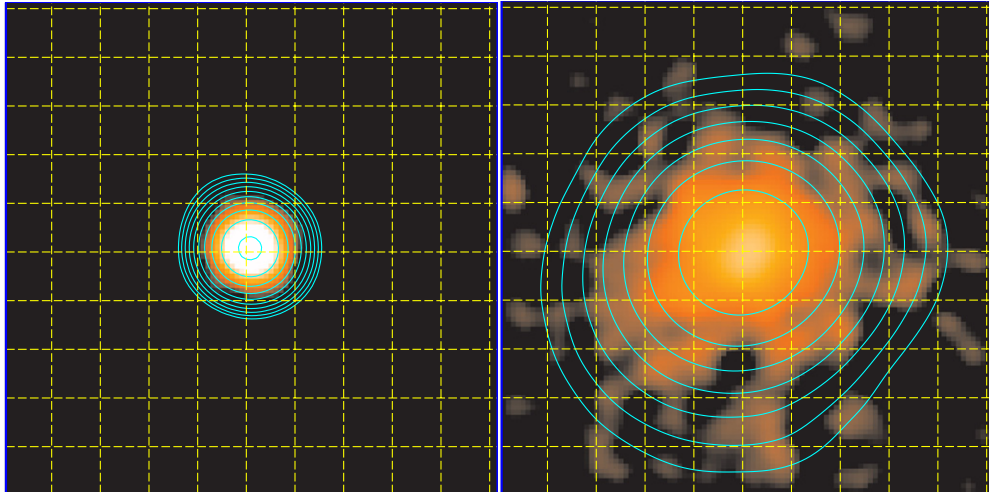


Figure 4. Left: scaled far-UV continuum image produced (as described in the text) from the average of 92 continuum-selected LBGs, drawn from three independent fields. The regions shown are $20''$ ($\simeq 160$ physical kpc at $z = 2.65$) on a side, with a grid spacing of $2''$. Right: the continuum-subtracted, stacked $\text{Ly}\alpha$ image for the same sample of galaxies. In both panels, the contours are logarithmically spaced in surface brightness with the lowest contour shown at $\simeq 2.5 \times 10^{-19} \text{ erg s}^{-1} \text{ cm}^{-2} \text{ arcsec}^{-2}$. (A color version of this figure is available in the online journal.)

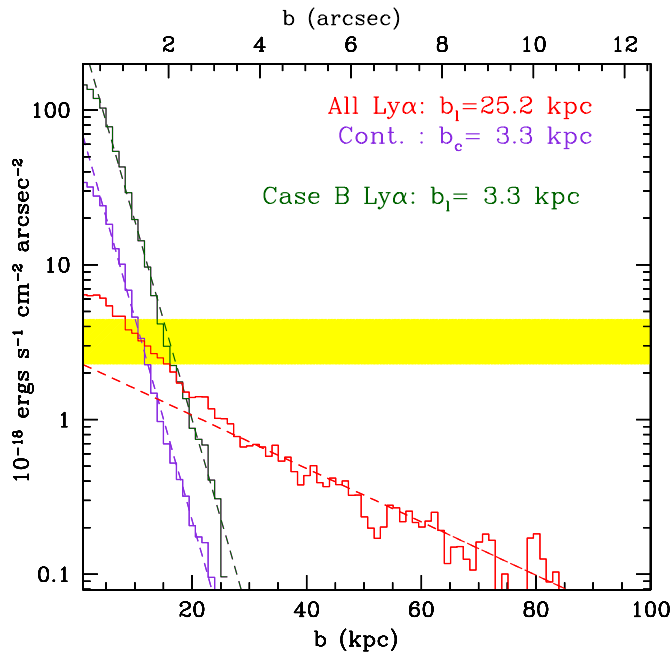


Figure 5. Observed average surface brightness profile for the 1220 \AA continuum light (blue) and the $\text{Ly}\alpha$ line (red) for the full sample of 92 continuum-selected galaxies, evaluated over the same rest-frame bandwidth sampled by the $\text{Ly}\alpha$ image (24.3 \AA). Note that these profiles are simply the azimuthal averages of the stacked images shown in Figure 4. The light-shaded region indicates the range of typical $\text{Ly}\alpha$ surface brightness threshold reached by deep $\text{Ly}\alpha$ surveys for the detection of individual objects. The dashed lines show the surface brightness profile assuming that $S(b) = C_i \exp(-b/b_i)$ with parameters given in Table 2. The corresponding angular scale at $\langle z \rangle = 2.65$ is given along the top axis. For the purpose of comparison, we also show the $\text{Ly}\alpha$ profile expected for the same sources under the assumption of the “Case B” $\text{Ly}\alpha$ to CB ratio, no destruction of $\text{Ly}\alpha$ by dust, and no spatial diffusion of $\text{Ly}\alpha$ photons due to resonant scattering (i.e., the $\text{Ly}\alpha$ and CB profiles would be identical in shape, and since $W_0(\text{Ly}\alpha) = 100 \text{ \AA}$, the $\text{Ly}\alpha$ line image would be a factor of $\simeq 4.1$ brighter than the continuum in the effective rest-frame bandwidth of 24.3 \AA).

(A color version of this figure is available in the online journal.)

(i.e., Case B), and $\text{Ly}\alpha$ and CB light had the same spatial distribution on average.

The surface brightness profiles for both the continuum and the $\text{Ly}\alpha$ line images are reasonably well-fit by an exponential

of the form $S(b) = C_i \exp(-b/b_i)$ for projected radii beyond the central arcsec; the parameters of the best-fit values for the normalization C_i and scale length b_i are given in Table 2 for each sub-sample as well. In the full image stack, the effective surface brightness detection thresholds are a factor of ~ 10 lower than for individual galaxies; it is clear that the distribution of $\text{Ly}\alpha$ emission is very different from that of the continuum for every sub-sample, with best-fit $\text{Ly}\alpha$ scale lengths of $b_l \simeq 20\text{--}30 \text{ kpc}$, compared with the corresponding continuum emission which has $b_c \simeq 3\text{--}4 \text{ kpc}$. It is important to note that the true difference in scale length is larger, since we have made no attempt to deconvolve the profiles from the seeing disk, which was $\text{FWHM} \simeq 0''.86, 1''.20, \text{ and } 0''.80$ for HS1549, HS1700, and SSA22a, respectively. The continuum profiles of the stacked composite CB images have $\text{FWHM} \simeq 1''.2\text{--}1''.4$, indicating average (seeing deconvolved) galaxy continuum sizes of $\text{FWHM} \simeq 0''.80$ ($\sigma \simeq 0''.35$). These deconvolved angular sizes are also consistent with measurements of similar galaxies in deep *Hubble Space Telescope*/Advanced Camera for Surveys images (e.g., Peter et al. 2007; Law et al. 2007).

The stacked $\text{Ly}\alpha$ and CB images as in Figures 5 and 6 represent unweighted averages of all galaxies in the sample (with masking as described above). This choice was motivated by the desire to preserve the photometric integrity of the stacks so that fluxes could be measured directly using aperture photometry, but also because any scaling or weighting would require deciding what the relevant figure of merit should be. Medians are often used to suppress outliers in stacked data sets, but they have the disadvantage for the present application of not preserving flux in two-dimensional images, of working best when scaling has been applied to individual images going into the stack, and of suppressing real signal as it approaches the noise level. Nevertheless, in Figure 7 we show a comparison of the surface brightness profiles for median-combined stacks as compared to mean-combined for both line and continuum.

We have argued that our sample of galaxies with $\langle z \rangle = 2.65$ has emission line and continuum properties characteristic of those in the full LBG spectroscopic surveys at these redshifts. Figure 8 shows that the diffuse $\text{Ly}\alpha$ emission is also consistent among the three survey fields taken individually. This is important, since each field samples galaxies at a different redshift

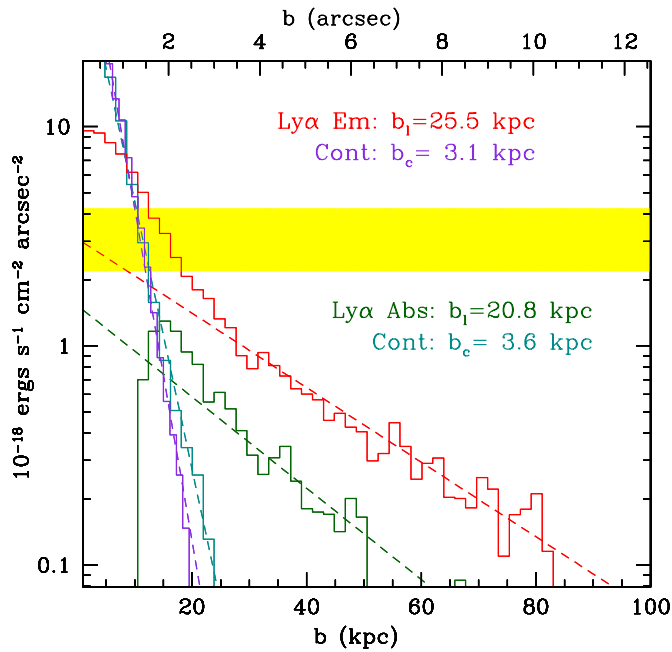


Figure 6. Same as Figure 5, comparing the average surface brightness profiles for the sample divided according to whether the NB measurements indicate net Ly α “Abs” or “Em.”

(A color version of this figure is available in the online journal.)

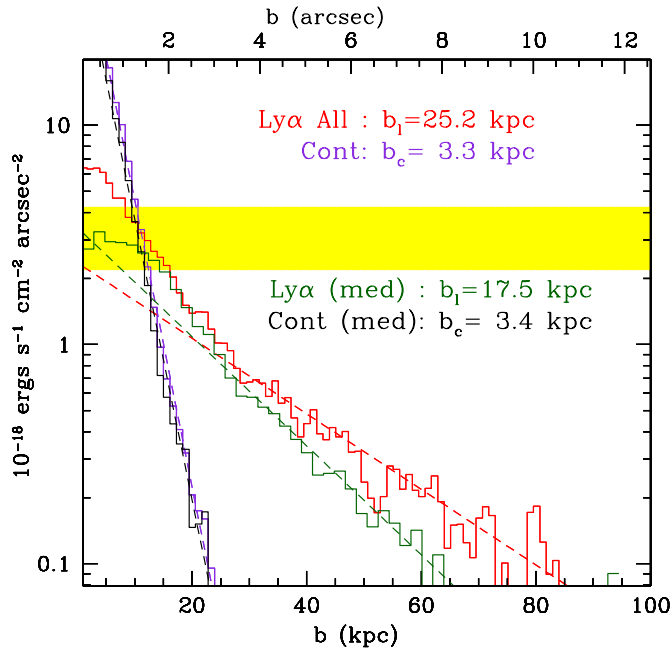


Figure 7. Same as Figure 5, comparing the surface brightness profile measured from median-combined rather than mean-combined stacks of Ly α and CB sub-images. Note that the line-to-continuum ratio is not necessarily preserved in the median stacks. The general effect of this alternative processing is to decrease the measured Ly α scale lengths by $\sim 25\%$, though the Ly α profiles remain much more extended than the continuum profiles.

(A color version of this figure is available in the online journal.)

with observations subject to a different set of conditions, using different telescope and instrument combinations. We also note that the bright QSO known to lie within the survey volume in

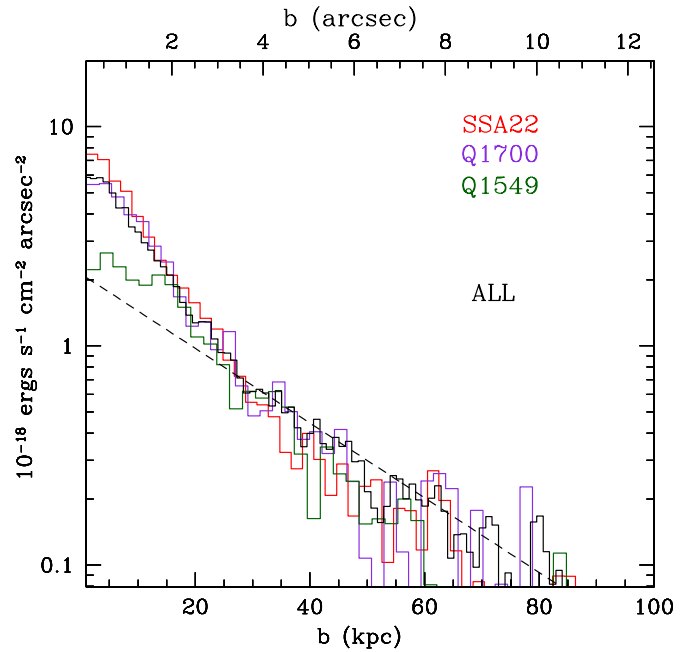


Figure 8. Average observed Ly α surface brightness profiles for galaxy sub-samples separated by field, as indicated. The Ly α profiles were scaled according to the relative continuum flux density in each field, for display purposes. The small differences in the mapping of angular scale to physical scale have also been removed to facilitate the comparison. The measured values of the average Ly α rest equivalent width are $\langle W_0(\text{Ly}\alpha) \rangle = 28.1 \text{ \AA}$, 28.6 \AA , and 42.0 \AA for HS1549, HS1700, and SSA22, respectively.

(A color version of this figure is available in the online journal.)

the HS1549 field appears not to have had a significant effect on the Ly α emission from the galaxies in our sample.²⁰

Figure 6 shows the measured surface brightness profiles and best-fit exponential parameters for the sub-sample with net Ly α emission (see the second row of Table 2). The profile of the Ly α Em composite is qualitatively similar to that of the full sample. The main difference is in the central Ly α surface brightness: Ly α Em objects have (on average) Ly α surface brightness well above the threshold for individual detection (light-shaded region in Figures 5 and 6) to projected distances of $b \sim 20\text{--}25$ kpc ($2''.5\text{--}3''.1$), whereas even the peak Ly α SB in the full sample (Figure 5) barely reaches the (individual) detectability threshold. Also illustrated in Figure 6 is the SB profile for the “Ly α Abs” sub-sample. The Ly α SB scale length for the Abs sample is still $\simeq 4$ times larger than for the corresponding continuum light (third row of Table 2) and has a comparable Ly α scale length b_l to that measured for the Ly α Em sample (second row of Table 2), albeit with a $\simeq 3$ times lower normalization for $b \gtrsim 20$ kpc. Clearly the difference is much larger for $b \lesssim 1''$, where the Abs sample exhibits a large “hole” in which Ly α absorption strongly dominates.

Figure 9 reproduces the SB profiles of the “Ly α Em” and “Ly α Abs” sub-samples together with the average profile of LAEs (green), and non-LAEs (cyan). The LAE sub-sample is very similar to that of the larger “Ly α Em” subset, but has an average SB a factor of ~ 1.5 higher for $b \gtrsim 10$ kpc

²⁰ The galaxy regions most likely to be affected by excess ionizing radiation from the QSO would lie in the outer parts; whether this radiation would increase or decrease the amount of Ly α emission from galaxies would depend on the physical state of the gas. The galaxies in the HS1549 field are fainter by about 30% on average (in terms of apparent continuum magnitude) than in the other two fields; the differences in the Ly α profiles on small scales may be a consequence of this selection issue.

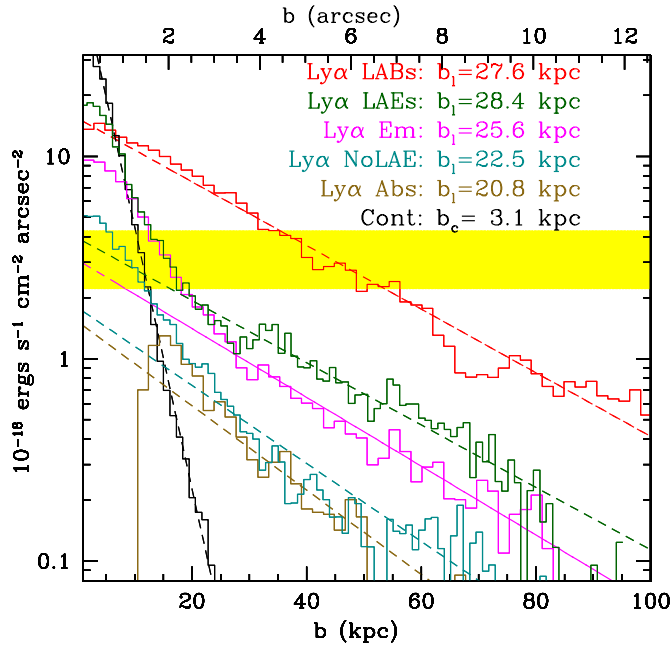


Figure 9. As for Figure 5, where here the $\text{Ly}\alpha$ radial SB profiles are shown for each of the sub-samples in Table 2, along with the exponential models for each. Also included for comparison is the average surface brightness profile of 11 giant $\text{Ly}\alpha$ “blobs” observed in the same three survey fields (red).

(A color version of this figure is available in the online journal.)

(and a factor $\simeq 3$ higher for $b \leq 10$ kpc). Also plotted for comparison (Figure 9) is the average SB profile of 11 LABs (see, e.g., Steidel et al. 2000; Matsuda et al. 2004), which for the present we define as $\text{Ly}\alpha$ -selected objects with detected isophotal diameters $d > 5''$, discovered in the same three survey fields. None of the 11 blobs are included in the main galaxy sample, since they do not have central continuum sources that satisfy the usual LBG color criteria. As indicated in Table 2, the blobs have an average $\text{Ly}\alpha$ luminosity $\simeq 7$ times higher than an average galaxy in our sample. It appears that even the most extreme LABs do not have fundamentally different SB profiles compared to those of typical galaxies in the sample *except* that their surface brightness normalization exceeds the typical detection threshold to $b \sim 50$ kpc ($\sim 6''$). In other words, if one were routinely sensitive to a surface brightness of $\sim 10^{-19} \text{ erg s}^{-1} \text{ cm}^{-2} \text{ arcsec}^{-2}$, all continuum-selected LBGs would be “blobs.”²¹ We will return to a more detailed discussion of $\text{Ly}\alpha$ demographics in Section 4.

If we assume for the moment that the extended $\text{Ly}\alpha$ halos represent photons originating in the galaxies’ H II regions, we can use the composite $\text{Ly}\alpha$ line and CB images to measure the integrated $\text{Ly}\alpha$ line-to-continuum ratio, usually parameterized as $W_0(\text{Ly}\alpha)$, the $\text{Ly}\alpha$ equivalent width. The total $\text{Ly}\alpha$ fluxes have been measured directly from the calibrated stacked images (Column 8 of Table 2); a comparison with the continuum flux density measured near the wavelength of $\text{Ly}\alpha$ from the CB images (Column 3 of Table 2) allows the calculation of $W_0(\text{Ly}\alpha, \text{tot})$ (Column 12). These numbers can be compared directly with the spectroscopic measurements (Column 11) for the same galaxy sub-samples. The values that include the diffuse $\text{Ly}\alpha$ extending to ~ 80 kpc radii around galaxies exceed the spectroscopically inferred $W_0(\text{Ly}\alpha, \text{spec})$ by an average factor

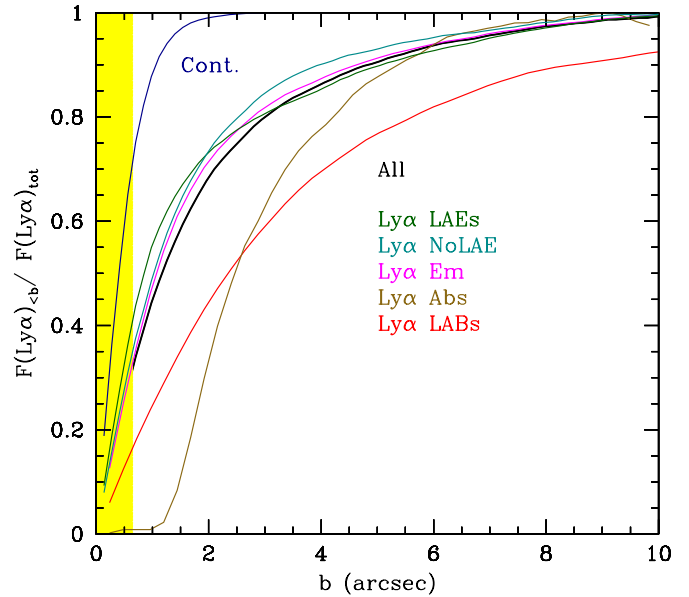


Figure 10. Cumulative fraction of the large-aperture $\text{Ly}\alpha$ flux as a function of angular aperture radius b for each galaxy sub-sample. The vertical dashed line drawn at $b = 0.65$ indicates the typical effective aperture for the slit spectra of the same objects. The dark blue curve corresponds to the cumulative continuum flux (for the stack of the full sample) as a comparison.

(A color version of this figure is available in the online journal.)

of $\simeq 5$ for the full galaxy sample. Figure 10 shows the cumulative fraction of the total $\text{Ly}\alpha$ flux as a function of aperture radius b (in arcseconds) for the galaxy samples in Table 2. It is interesting to note that including the spatially extended $\text{Ly}\alpha$ emission brings the average galaxy into the range that would nominally qualify as an LAE ($W_0(\text{Ly}\alpha) > 20 \text{ \AA}$)—even for the “non-LAE” sub-sample that explicitly *excludes* the 18 conventional LAEs (fourth row of Table 2).

One can also compare the measured large-aperture $W_0(\text{Ly}\alpha)$ with expectations for the $\text{Ly}\alpha$ to continuum ratio for Case B recombination and no dust. As discussed above, an asymptotic value of $W_0(\text{Ly}\alpha) \simeq 100 \text{ \AA}$ is expected when star formation has been continuous for $t_{\text{SF}} \gtrsim 4 \times 10^7 \text{ yr}$.²² Note that approximately the same value of $W_0(\text{Ly}\alpha)$ is expected as long as $\text{Ly}\alpha$ photons do not suffer greater attenuation by dust than continuum photons just off the $\text{Ly}\alpha$ resonance. Thus, the fact that most of the values of $f_{\text{esc,rel}} \equiv W_0(\text{Ly}\alpha)/100 \text{ \AA}$ (Table 3) are significantly smaller than unity means that $\text{Ly}\alpha$ photons suffer greater extinction than the continuum, by factors ranging from 1.1 to 6.0 with an average $\simeq 2.8$ for the full sample of 92 galaxies.

We note that the values in Table 3 for $f_{\text{esc,rel}}$ have been obtained using a method that appears to differ from that used in some recent work (e.g., Gronwall et al. 2007; Nilsson et al. 2009; Kornei et al. 2010). Most estimates of $f_{\text{esc,rel}}$ use stellar population synthesis models to estimate the level of extinction, which is then used to derive SFR to calculate the expected $\text{Ly}\alpha$ luminosity based on the assumption of Case B recombination and the form of the stellar IMF. While we are using largely identical spectral energy distribution (SED) modeling to estimate $\text{SFR}_{\text{UV,corr}}$, we use the observed $W_0(\text{Ly}\alpha)$ as a direct observational estimate of $f_{\text{esc,rel}}$. The present method relies on the same assumptions about the stellar IMF (i.e., based on a Salpeter-like IMF for high-mass stars) to estimate the $\text{Ly}\alpha$

²¹ Conversely, if the LABs were several times less luminous but had the same surface brightness profile, they would fail to be recognized as “blobs” at all.

²² The typical inferred age for galaxies similar to those in the present sample is $\sim 500 \text{ Myr}$ (e.g., Shapley et al. 2005; Reddy et al. 2008).

Table 3
Inferred Continuum and Ly α Attenuation for Sub-samples

Sample ^a	$m_{\text{AB,med}}/\langle m_{\text{AB}}(1500\text{ \AA}) \rangle^b$	$E(B - V)_{\text{med}}^c$	SFR_{UV}^d	$\text{SFR}_{\text{UV,corr}}^e$	$f_{\text{esc}}(\text{UV})^f$	$f_{\text{esc,rel}}(\text{Ly}\alpha)^g$	$f_{\text{esc,tot}}(\text{Ly}\alpha)^h$	$A(\text{Ly}\alpha)/E(B - V)^i$
All (92)	24.47/24.50 \pm 0.55	0.17	6.3	34.3	0.17	0.36	0.061	17.9
Ly α Em (52)	24.50/24.55 \pm 0.56	0.11	6.0	18.6	0.32	0.45	0.144	19.1
Ly α Abs (40)	24.44/24.43 \pm 0.54	0.19	6.6	46.5	0.14	0.17	0.024	21.3
All non-LAE (74)	24.43/24.42 \pm 0.54	0.18	6.7	42.6	0.16	0.29	0.046	18.5
LAE only (18)	24.85/24.80 \pm 0.50	0.09	4.5	11.3	0.40	0.93	0.372	11.9

Notes.

^a Galaxy sub-sample, drawn from the full sample (all) of 92 continuum-selected galaxies with Ly α imaging. The details of the sub-samples are described in the text.

^b Median and mean/standard deviation of continuum apparent magnitude at $\lambda_0 \simeq 1500\text{ \AA}$

^c Median $E(B - V)$ inferred from SED fitting.

^d Median SFR, in $M_{\odot}\text{ yr}^{-1}$, from UV continuum with no dust correction.

^e Median SFR after correction based on $E(B - V)$ and Calzetti et al. (2000) reddening relation.

^f Fraction of 1500 \AA photons escaping galaxy.

^g Relative escape fraction of Ly α photons, $\equiv W_0(\text{Ly}\alpha)_{\text{tot}}/100\text{ \AA}$.

^h Fraction of Ly α photons escaping, $f_{\text{esc,tot}} = f_{\text{esc,rel}} \times f_{\text{esc}}(\text{UV})$.

ⁱ Ratio of attenuation of Ly α photons to $E(B - V)$ when both are expressed in magnitudes.

photon production rate per unit star formation; the difference is that we rely on the ratio of Ly α photon production to that of $\lambda_0 \simeq 1220\text{ \AA}$ continuum photons from the same ensemble of stars. The advantage of using the equivalent width measurement is that it should be independent of extinction if Ly α and $\simeq 1220\text{ \AA}$ continuum photons experience the same attenuation, and would directly reflect the relative attenuation of line and continuum if $A_{\text{Ly}\alpha} \neq A_{1220}$. Because both of these methods rely on measuring the integrated Ly α line flux, an underestimate of Ly α relative to the continuum will cause $f_{\text{esc,rel}}$ to be underestimated by the same factor. For the present purposes, we prefer using the method relying on $W_0(\text{Ly}\alpha)$ since it depends on a largely independent measurement that may avoid propagating possibly large systematic errors in the estimates of $E(B - V)$ from SED fitting (or from the assumed extinction curve, which relates $E(B - V)$ to $A(\lambda)$) to the calculation of $f_{\text{esc,rel}}$. In general, we expect that the undercounting of Ly α photons due to the aperture effects discussed above are likely to dominate any differences in inferred $f_{\text{esc,rel}}$.

Column 10 of Table 2 compiles the average Ly α luminosity $L_{\text{tot}}(\text{Ly}\alpha)$ implied by the measured value of $F_{\text{tot}}(\text{Ly}\alpha)$ assuming the sample mean redshift $\langle z \rangle = 2.65$. If one naively converts these numbers to an equivalent SFR (i.e., divide by $2 \times 10^{42}\text{ erg s}^{-1}$ to yield SFR in units of $M_{\odot}\text{ yr}^{-1}$) the results range from 2.1–11.8 $M_{\odot}\text{ yr}^{-1}$ for the various sub-samples, with an average of 3.1 $M_{\odot}\text{ yr}^{-1}$ for the full sample. In Table 3 we have compiled the statistics of the far-UV inferred SFRs and continuum extinction for each of the sub-samples from Table 2. The extinction estimates are parameterized by $E(B - V)$ and assume the Calzetti et al. (2000) starburst attenuation curve; $E(B - V)$ was estimated from SED fits when available, and using the far-UV continuum slope for the $\sim 20\%$ of galaxies lacking adequate near-IR photometric coverage for SED fitting. In the context of the assumed starburst attenuation relation, the extinction (in magnitudes) at 1500 \AA is $A(1500\text{ \AA}) = 11.16 E(B - V)$ (Meurer et al. 1999; Calzetti et al. 2000; Reddy et al. 2006, 2010). The UV continuum magnitudes near rest-frame 1500 \AA were used to estimate SFR_{UV} (e.g., Madau et al. 1998; Steidel et al. 1999; Adelberger & Steidel 2000) with a median value of $\langle \text{SFR}_{\text{UV}} \rangle \simeq 6.3 M_{\odot}\text{ yr}^{-1}$. Applying the median $E(B - V)$ to the median SFR_{UV} within each sub-sample implies that $11.3 M_{\odot}\text{ yr}^{-1} \lesssim \langle \text{SFR}_{\text{UV,corr}} \rangle \lesssim 46.5 M_{\odot}\text{ yr}^{-1}$, with an overall median of

$\text{SFR}_{\text{UV,corr}} = 34.3 M_{\odot}\text{ yr}^{-1}$ —very close to the mean of the LBG sample observed in H α by Erb et al. (2006b) and consistent with the mean bolometric luminosity of identically selected LBGs estimated using multiple SFR indicators (Reddy et al. 2006, 2010). The median $E(B - V)$ varies considerably among the sub-samples, so that the median attenuation of the UV continuum is inferred to range from $\simeq 2.5$ for the LAEs to $\simeq 7$ for the Ly α Abs sub-sample. In Table 3 we list the inverse of this factor, which we have called $f_{\text{esc}}(\text{UV}) \equiv \text{SFR}_{\text{UV}}/\text{SFR}_{\text{UV,corr}}$. Our estimate of the fraction of all Ly α photons produced by photoionization in the galaxy H II regions that have been detected is then given by $f_{\text{esc,tot}}(\text{Ly}\alpha) \equiv f_{\text{esc,rel}}(\text{Ly}\alpha) \times f_{\text{esc}}(\text{UV})$. These values range from $f_{\text{esc,tot}}(\text{Ly}\alpha) \simeq 0.37$ for the LAE sub-sample to $f_{\text{esc,tot}}(\text{Ly}\alpha) \simeq 0.024$ for the “Ly α Abs” sub-sample. The average for the entire sample is $f_{\text{esc,tot}}(\text{Ly}\alpha) \simeq 0.061$. We note that this fraction is close to the average value of $f_{\text{esc}}(\text{Ly}\alpha)$ estimated by Hayes et al. (2010) based on a very different approach involving a comparison of H α and Ly α luminosity density at $z \simeq 2.2$.

The last column of Table 3 shows the inferred ratio $A(\text{Ly}\alpha)/E(B - V)$, where both quantities are expressed in magnitudes and $E(B - V)$ is inferred from the stellar SED. The numeric value of this ratio is $\simeq 19.5 \pm 1.5$ for all sub-samples except the LAEs, which have $A(\text{Ly}\alpha)/E(B - V) \simeq 11.9$. Since the Calzetti et al. (2000) extinction curve predicts that the UV continuum near the Ly α line has $A(1220\text{ \AA})/E(B - V) \simeq 12$, it seems that Ly α emission from the LAEs drawn from our LBG sample exhibit no evidence for selective extinction of Ly α photons, while for other LBGs the attenuation $A(\text{Ly}\alpha)$ is ~ 1.6 times higher than for continuum photons for the same value of $E(B - V)$. If the Ly α escape fraction is controlled by processes confined to H II regions, the result suggests that $E(B - V)_{\text{neb}} \simeq \eta E(B - V)_{\text{stars}}$ with $\eta \simeq 1.6$, on average. This can be compared with the relationship inferred for nearby star-forming galaxies, $\eta \simeq 2.5$, based on measurements of the Balmer decrement (Calzetti et al. 2000). At present, there are few galaxies for which Ly α , H α , and H β have all been measured, though there are some indications that the same value of $E(B - V)$ applies for both continuum starlight and H α for galaxies similar to those in the current sample (Erb et al. 2006a; but see Förster Schreiber et al. 2009 for possibly conflicting evidence).

4. IMPLICATIONS OF DIFFUSE Ly α HALOS

Diffuse Ly α emission from the outer parts of actively star forming galaxies is an unavoidable consequence of a gaseous CGM so long as some component of it is optically thick to Ly α photons and some fraction of Ly α photons initially produced in H II regions are not absorbed by dust at smaller galactocentric radii. Calculation of the emergent Ly α emission is undoubtedly complex, since it will depend on the details of the gas-phase structure and kinematics as well as the relative distribution of the sources (e.g., H II regions) and the sinks (e.g., dust) of Ly α photons. A fully successful model requires three-dimensional radiative transfer calculations and all of the relevant spatial and kinematic information as input. Such a treatment is far beyond the scope of this paper; however, it is interesting to ask whether the spatial profiles of Ly α emission from the same star-forming galaxies can be understood in the context of a schematic model. In this section, we describe such a model that begins with inferences on the structure and kinematics of CGM gas from S2010, and then test for consistency with both the Ly α emission observations and the absorption-based S2010 CGM model.

4.1. A Model for Ly α Scattering Halos

We first consider the probability that an Ly α photon produced in a galaxy's central few kpc will escape in the direction of a particular observer's line of sight. The escape probability will depend on the kinematics and optical depth distribution of the CGM gas, and so one might expect it to be closely related to the characteristics of absorption lines observable both in the galaxy spectra themselves ($b \lesssim 2\text{--}3$ kpc) and in lines of sight to background objects with at larger impact parameter $b \gg 0$. The conditions necessary for an Ly α line photon to escape in the direction of a particular observer are: (1) it must either be emitted at a frequency that is well off resonance for any H I in the foreground (i.e., between the point of emission and the observer) and/or (2) it must be scattered in a direction that happens to have low spatial covering fraction f_c of H I.²³

For extended Ly α produced by scattering in a gaseous halo, the observed surface brightness profile $S(b)$ will then be related to the integral along the line of sight at impact parameter b of the product of (1) the Ly α photon density, (2) the probability that an Ly α photon will be scattered in our (the observer's) direction, and (3) the probability that once scattered in our direction a photon will proceed to escape the nebula before being scattered once again. The situation is somewhat analogous to the galaxy outflow model used to match absorption line equivalent widths W_0 versus impact parameter b presented in S2010. Figure 11 shows the assumed geometry (cf. Figure 23 of S2010.) In the absorption case, a line of sight to a background object pierces the radial flow at projected distance b , and the resulting absorption line strength is modulated by the integral along the line of sight of the quantity $1 - f_c(r, v_{\text{out}})$, where r is the galactocentric radius and $v_{\text{out}}(r)$ is the flow velocity at radius r . As discussed by S2010, the velocity field in the absorbing gas can have a large effect on the strength of absorption lines in the spectra of background sources when the transition is saturated, even if the covering fraction is significantly smaller than unity. S2010 argued that consistency between the absorption line strength as a function of impact parameter on one hand, and the strength and profile shape of lines observed in the spectra of the galaxies themselves on the other, requires large velocities

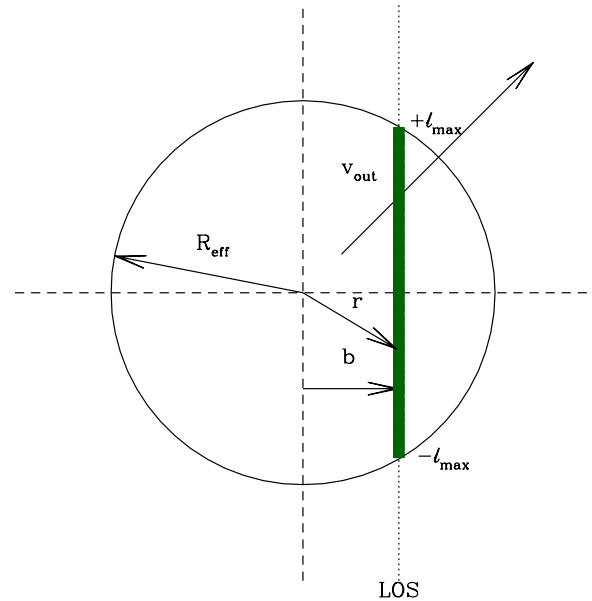


Figure 11. Coordinate system for the schematic model of scattered Ly α emission from galaxies, where b is the line-of-sight impact parameter, r is the galactocentric distance, and R_{eff} is the assumed physical size of the scattering medium. In the model, Ly α photons are produced near $r \sim 0$, after which they diffuse outward until they are either destroyed or they escape the scattering medium. The covering fraction of gas at galactocentric radius r is assumed to be of the form $f_c(r) \propto r^{-\gamma}$ (see also S2010).

(A color version of this figure is available in the online journal.)

and velocity gradients in the gas. The absorption cross section is dominated by *outflowing* material, and the flows are inferred to be clumpy (i.e., multi-phase), with both high- and low-ionization ionic species observed over similar ranges of velocity and galactocentric distance. In the context of the CGM model, most of the acceleration of cool gas to high velocity occurs in the inner several kpc. The covering fraction f_c of gas giving rise to absorption in a particular transition decreases with increasing galactocentric distance r , modeled as a power law of the form $f_c \propto r^{-\gamma}$.

In general, the larger the range of gas-phase bulk velocity sampled along the observer's line of sight at impact parameter b , the greater the chance will be that a scattered Ly α photon will reach the observer without further scattering. For simplicity, in our model we assume that all scattering events are isotropic, and that the gas-phase velocity field is axisymmetric and is a monotonic function of galactocentric distance r (see S2010 for a justification of this assumption). If the bulk velocity field in the outflow has a range and amplitude much larger than that of the local velocity dispersion in the H I gas,²⁴ or when $f_c \ll 1$, the problem can be reduced to a geometric one in which the covering fraction depends only on galactocentric radius r , $f_c = f_c(r)$. Clearly, it would be interesting to measure the velocity field of extended Ly α emission in order to gauge the role kinematics play in the transfer of Ly α photons. Unfortunately, beyond the central, high surface brightness regions there are few constraints on the line shapes, and at present we have only

²³ In the limit of no H I gas outside of a galaxy's H II regions, the emergent Ly α line would have roughly the same spatial extent as that of the UV continuum.

²⁴ In the models discussed here, this is assumed to be the case based on the results presented in S2010. While velocity is not used explicitly as a model parameter, large velocity gradients along the line of sight directly affect the probability that a scattered Ly α photon will ultimately escape. In other words, the effective covering fraction of optically thick H I as seen by an Ly α photon emitted from a particular position in the CGM implicitly includes an integral over velocity even if it is not explicitly used as a model parameter. See Steidel et al. (2010) for a more detailed discussion of this issue.

(projected) spatial information integrated over the full range of velocity.

When considering emission (rather than absorption in the spectra of background objects), one needs to account for the Ly α “source function” which varies with spatial position, as well as variations in opacity parameterized by $f_c(r)$. The Ly α photon density available to contribute to the observed $S_{\text{Ly}\alpha}(b)$ will depend on the fraction of Ly α photons that have been able to diffuse outward to $r \gtrsim b$, which may be only a small fraction of the Ly α photons initially produced by recombination in H II regions. When the covering fraction is high at small radii, one would expect the emergent Ly α emission from that region to be suppressed—photons are either destroyed or radiatively trapped until they make their way to locations from which escape is more probable. The flux of Ly α photons (assumed to be produced at small r at a \sim constant rate related to the SFR) at galactocentric radius r will be reduced by an overall geometric factor $1/4\pi r^2$, and by the destruction of Ly α via absorption by dust grains.²⁵

This diminished Ly α radiation field would produce no Ly α halo at $b > r$ if $f_c(r) = 0$ because photons would appear to be released from an Ly α “photosphere” that would approximately extend to the edge of the gas distribution. The apparent outer edge of the Ly α scattering halo should correspond to the radius at which f_c becomes negligible and the scattered component of Ly α falls below the observational threshold. At small radii, where $f_c(r) = 1$ and the optical depth encountered in any direction is substantial (e.g., for galaxies having absorption-dominated continuum spectra), Ly α photons will be resonantly trapped for a large number of scattering events before diffusing spatially outward. Most of the dust absorption, if present, would be expected to occur in such regions. Once $f_c(r)$ falls below unity at larger radii, Ly α photons that have not been destroyed may be scattered in the observer’s direction. Thus, the relative rate of Ly α scattering events at radius r will be $\propto f_c(r)/4\pi r^2$ where $f_c(r)$ is the H I covering fraction. The chance that a scattered Ly α photon will be emitted in the observer’s direction (without any further interactions prior to escape) increases with decreasing characteristic f_c , with probability roughly $\propto [1 - f_c(r)]$ for $f_c(r) \leq 1$. The Ly α surface brightness as seen by an observer in a particular direction will then be proportional to the product of these two terms, integrated along the line of sight through the galaxy at impact parameter b :

$$S_{\text{Ly}\alpha}(b) \propto S_0 \int_{-l_{\text{max}}}^{+l_{\text{max}}} \frac{f_c(r)[1 - f_c(r)]}{4\pi r^2} dl, \quad (2)$$

where l is the coordinate distance along the observer’s line of sight at impact parameter b , $l_{\text{max}} = (R_{\text{eff}}^2 - b^2)^{1/2}$, S_0 is a normalization for the surface brightness distribution, and R_{eff} is the effective size of the scattering halo (see Figure 11). Note that the integrand tends toward zero when $f_c(r) \simeq 1$, qualitatively accounting for the suppression of Ly α emission in regions with high $f_c(r)$. Clearly, when $f_c = 1$ the purely geometric model is no longer valid because the Ly α emission intensity associated with an optically thick region can be “negative,” i.e., there is a net removal of Ly α photons at that spatial position that will reduce the net surface brightness along that particular line of sight.

In the S2010 CGM model, the radial dependence of the covering fraction of gas was found to be consistent with a power

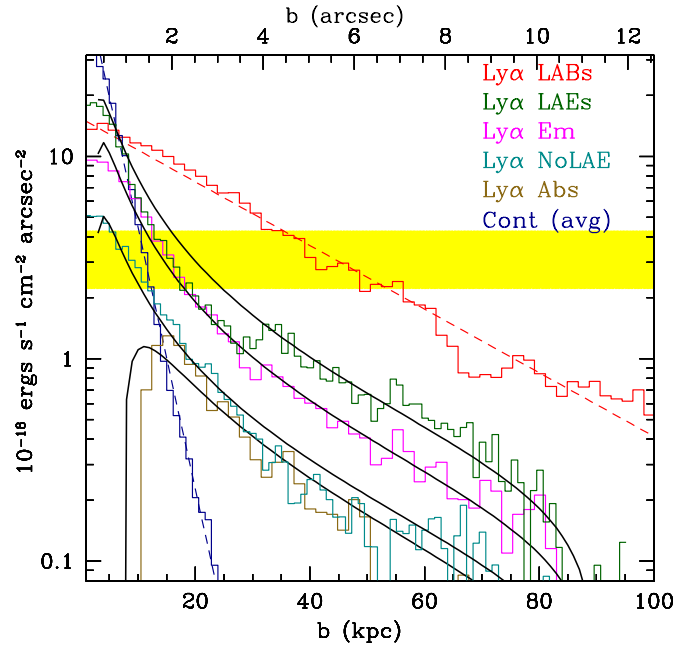


Figure 12. Same as Figure 9, but where models described by Equation (2) have replaced the exponential profile used in Figure 9. Parameters for the four model curves shown are summarized in Table 4. All four model curves have $R_{\text{eff}} = 90$ kpc and $f_c(r) \propto (r/r_0)^{-\gamma}$ with $\gamma \simeq 0.6$ – 0.8 . The “Ly α Abs” model produces a central hole in the Ly α emission by adjusting the normalization of f_c with the parameter r_0 ; the larger value of r_0 indicates that the CGM remains optically thick to Ly α photons to larger galactocentric radii than for the other sub-samples.

(A color version of this figure is available in the online journal.)

law of the form $f_c(r) \propto r^{-\gamma}$, where $0.3 \lesssim \gamma \lesssim 0.6$ depending on the ionization state of the tracer ion; $f_c(r)$ becomes consistent with zero for $r > R_{\text{eff}} \sim 90$ kpc for most of the observed ions. If we take the power-law form for f_c (with index γ) characteristic of the highest H I optical depth material, Equation (2) can be used to predict $S_{\text{Ly}\alpha}(b)$ given an overall normalization S_0 , a characteristic radius r_0 at which $f_c(r)$ first falls below unity (i.e., $f_c(r) = (r/r_0)^{-\gamma}$), and the effective size of the scattering medium, R_{eff} . We account qualitatively for the variation of the spatial profile of Ly α emission in the central regions of a galaxy by (artificially) allowing $f_c > 1$ at $r < r_0$, using an extrapolation of the same power-law form for $f_c(r)$. Since the integrand becomes negative when $f_c > 1$, this leads to suppression of the Ly α surface brightness for any line of sight that intercepts such a region. In practice, the central Ly α emission must be substantially suppressed to match the observed profiles of any of the galaxy subsets, including the LAEs (cf. Figure 5).

Figures 12 and 13 show example models based on Equation (2) compared with the observed composite Ly α surface brightness profiles; the corresponding model parameters are given in Table 4. The overall shape of the predicted SB profile is sensitive to the value of γ parameterizing the radial dependence of the covering fraction of H I; $\gamma < 0.3$ produces Ly α profiles that are flatter than observed, while $\gamma > 0.8$ predicts Ly α emission which falls too rapidly with increasing b (Figure 13). As discussed above, the shape of the central portion of $S_{\text{Ly}\alpha}(b)$ is modulated by adjusting the galactocentric radius r_0 where $f_c(r_0) = 1$ (i.e., r_0 serves as a normalization of the maximum covering fraction). The presence of a central “hole” in $S_{\text{Ly}\alpha}(b)$ (as observed for the Ly α Abs sub-sample in Figure 12) can be reproduced by increasing r_0 so that the transition from net Ly α absorption to net Ly α emission moves to larger galactocentric

²⁵ Under the assumption of spherical symmetry, Ly α photons scattered at smaller radii are returned to the “pool” of Ly α photons potentially available for scattering at larger radii.

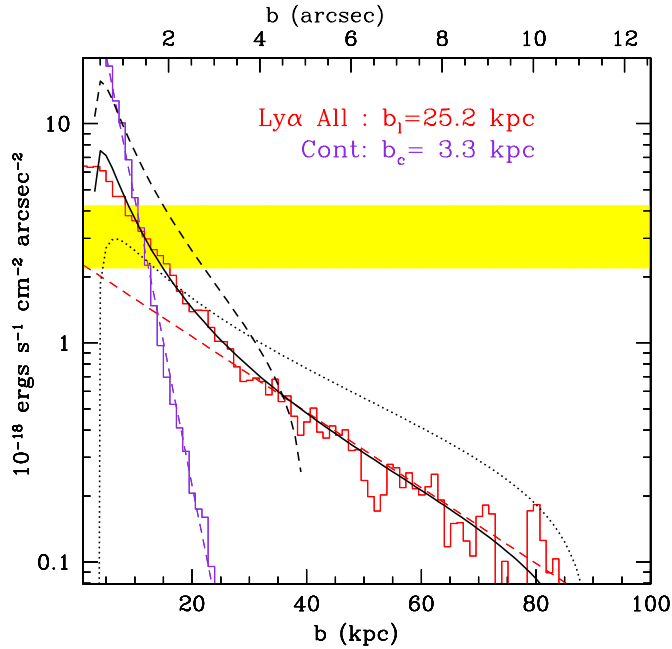


Figure 13. Same as Figure 5, where the preferred model is drawn with the solid black curve, corresponding to $S_0 = 11.5 \times 10^{-18} \text{ erg s}^{-1} \text{ cm}^{-2} \text{ arcsec}^{-2}$, $R_{\text{eff}} = 90 \text{ kpc}$, $r_0 = 2.2 \text{ kpc}$, and $\gamma = 0.6$, for covering fraction parameterized as $f_c(r) \propto (r/r_0)^{-\gamma}$ (see also S2010). The dashed curve shows a model with the same parameters, except $R_{\text{eff}} = 50 \text{ kpc}$, while the dotted curve assumes $\gamma = 0.2$, with all other parameters as they are for the preferred model.

(A color version of this figure is available in the online journal.)

radius. Once Ly α has a finite probability of escape (i.e., where $f_c(r) < 1$ in the context of our simple model), the residual Ly α photons at $r > r_0$ become available for redirection toward an external observer who then perceives the photon being “emitted” from a position at impact parameter b in projection.

The values of γ required to produce model profiles in reasonable agreement with their observed counterparts (Table 4 and Figure 12) are near the high end of the range inferred from the behavior of absorption line strength W_0 versus impact parameter b (S2010). One possible explanation for slightly steeper profiles is that the emission models assume *no* Ly α photons are destroyed once they propagate beyond $r \simeq r_0$; if Ly α has a finite chance of being absorbed by dust at $r > r_0$, the additional attenuation of Ly α would manifest itself as a steepening of the profile with respect to the pure scattering model. That the Ly α Abs model exhibits both the steepest decline in Ly α surface brightness ($\gamma \simeq 0.8$ compared with $\gamma \simeq 0.6$ for the other sub-samples) and the largest global extinction correction (Section 3 and Table 3) suggests that dust may not be confined solely to the central regions in such galaxies.

The model of the CGM proposed by S2010 almost certainly does not provide a unique explanation for the IS absorption line strength and kinematics as observed in the spectra of background galaxies; however, we have shown, with a simple extension of the model, that scattering of Ly α photons from the same CGM gas can also account for Ly α emission with radial surface brightness profiles and physical extent consistent with the observations. Regardless of the model details (which admittedly could be incorrect), the very similar physical scales involved ($R_{\text{eff}} \simeq 90 \text{ kpc}$) suggest a close causal connection between the cool gas observed to produce strong H I and low-ionization metallic absorption lines in the spectra of background

Table 4
Parameters for Model Ly α Spatial Profiles

Sample ^a	S_0 ^b	r_0 (kpc) ^c	γ ^d	R_{eff} (kpc) ^e
All	11.5	2.2	0.6	90
Ly α Em	17.0	2.0	0.6	90
Ly α Abs	4.5	5.9	0.8	90
All non-LAE	7.0	2.0	0.6	90
LAE only	25.0	1.9	0.6	90

Notes.

^a Galaxy sub-sample, drawn from the full sample (all) of 92 continuum-selected galaxies with Ly α imaging.

^b Intensity normalization for model (see Equation (2)), in units of $10^{-18} \text{ erg s}^{-1} \text{ cm}^{-2} \text{ Hz}^{-1}$.

^c Galactocentric radius at which $f_c = 1$

^d Power-law index in the radial behavior of the covering fraction, $f_c = (r/r_0)^{-\gamma}$.

^e Effective size of CGM region producing detectable Ly α emission, in kpc.

continuum sources, and spatially extended Ly α emission from the same host galaxies.

4.2. Comparison with Ly α Emission in Simulations

A scenario in which extended Ly α emission around galaxies is *dominated* by the scattering of Ly α photons initially produced inside the galaxies, rather than by external processes, has been the focus of a number of recent galaxy models including treatment of Ly α radiative transfer (e.g., Verhamme et al. 2008; Laursen et al. 2009a, 2009b; Zheng et al. 2010a, 2010b; Barnes et al. 2011). Each of these studies places emphasis on different aspects of the model galaxies, and cursory examination suggests a qualitative similarity to the observations presented here, since Ly α scattering leads to the spatial redistribution of the Ly α emission as seen by an observer. Gas-phase kinematics play a large role in determining how much Ly α emission escapes the galaxies, and in all of the models except those of Verhamme et al. (2008, which do not explicitly consider the spatial distribution of Ly α emission) the dominant velocity field is associated with infall/accretion. The predicted Ly α line profiles tend to be asymmetric and sometimes double peaked, usually dominated by photons that are blueshifted with respect to the galaxy systemic velocity—a configuration that is very rarely observed in galaxy spectra (e.g., Pettini et al. 2000; Shapley et al. 2003; Steidel et al. 2010). Also, while the three-dimensional models all produce Ly α emission that is significantly more extended than the UV continuum, the predicted surface brightness profiles of scattered emission generally declines much more rapidly than for the observed LBG Ly α halos (i.e., most would fall well below the current surface brightness limit). Barnes et al. (2011) have pointed out that higher outflow velocities tend to produce more extended Ly α emission in the context of their models, which include both inflows and outflows of gas, so that perhaps the missing ingredient is the presence of higher velocity outflows than have generally been modeled.

Most of the simulations work on Ly α emission from galaxies has not highlighted the potential utility of using Ly α emission observations as a means of revealing gas-phase structure in the surrounding CGM and IGM. One exception is a series of recent papers exploring how very sensitive NB observations of Ly α emission can be used along with cosmological simulations (including detailed radiative transfer) to trace the underlying large-scale structure at high redshifts (Zheng et al. 2010a, 2010b). In Zheng et al. (2010b), the authors explicitly calculate

the expected properties of diffuse Ly α emission around star-forming galaxies, with principal focus on LAEs at $z \simeq 6$. Like the scenario we have described above, the models assume that the ultimate source of the Ly α photons seen in emission is the galaxy H II regions, with extended emission resulting from the details of the Ly α radiative transfer. Zheng et al. (2010b) predict that the surface brightness profile surrounding individual galaxies will have two distinct components related closely to (1) the “halo exclusion scale” within comoving distances of $0.3 h^{-1}$ Mpc ($b \simeq 60$ physical kpc at $z \simeq 6$) and (2) a larger scale component arising from galaxy clustering, extending to $\simeq 3$ Mpc (comoving), or $\simeq 400$ physical kpc at $z \simeq 6$. The smaller scale is similar to the virial radius of the characteristic dark matter halos being considered in the simulation.²⁶ It is not completely straightforward to move the predictions to $z \simeq 2.65$ for comparison with our observations, but (as discussed in S2010) the CGM scattering medium observed around $z \sim 2$ –3 galaxies (which we have argued is responsible for absorption against background sources as well as for the extent of scattered Ly α emission) also has a size similar to the virial radius $r_v \simeq 80$ –100 kpc. However, it is not clear that the observations are consistent with the predictions when it comes to the dependence of the Ly α emission halo on other properties of the galaxies. In the Zheng et al. (2010b) models, the primary driver of the surface brightness profile is the gas-phase kinematics of the CGM gas; the characteristic scale of the inner component of Ly α emission relates to the “infall” region for the halo, within which gas is accreting onto the central galaxy (the simulations do not have outflowing material, and it is the kinematics of infalling material that modulate the escape of Ly α photons). On the other hand, in our picture the characteristic scale is related to the radial dependence of the covering fraction of neutral material and the gas-phase kinematics (assumed to be dominated by outflows). Within our sample of LBGs, the stacked Ly α images of various subsets indicate a rather consistent exponential scale length of $b_l \simeq 25$ kpc with at most a weak dependence on Ly α or UV luminosity or on the fraction of Ly α photons that escape the galaxy ISM. If there is a trend, it is in the direction opposite to that expected in the models.

Interestingly, many recent theoretical investigations focusing primarily on diffuse and extended Ly α from the outer parts of galaxies or LAEs have deliberately neglected the scattering of Ly α from the inside out (Dijkstra et al. 2006; Dijkstra & Loeb 2009; Kereš et al. 2009; Faucher-Giguere et al. 2011; Goerdt et al. 2010). Instead, attention has been drawn to Ly α emission associated with gas cooling as it accretes onto galaxies (“Ly α cooling”), or on Ly α fluorescence as a means of measuring the intensity of sources of ionizing photons at high redshifts. Both of these processes are discussed in Section 5.

In any case, there is no doubt that radiative transfer calculations will be key to a full understanding of diffuse Ly α emission from galaxies. However, it is essential that the CGM gas distribution and kinematics in the simulations match real galaxies. Without the correct gas-phase model, even the most sophisticated treatment of radiative transfer cannot yield a realistic result. The observations suggest that possibly important ingredients include a CGM that is clumpy on small scales and has

very large (non-gravitational) velocity gradients dominated by galaxy-scale outflows.

5. DISCUSSION

We have shown above that, on average, LBGs with far-UV luminosities $0.3 \lesssim (L/L_{UV}^*) \lesssim 3$ at $\langle z \rangle = 2.65$ exhibit spatially extended Ly α emission to physical radii of at least 80 kpc ($10''$), even when Ly α appears only in absorption for regions coincident with the UV continuum starlight. Figures 5, 6, and 12 show that the profiles of the Ly α emission are quite similar in shape independent of the spectral morphology, with the main difference being the overall intensity normalization and the presence or absence of emission spatially coincident with the continuum light (i.e., the inner ± 5 kpc). The observations suggest that the Ly α -scattering CGM may be statistically universal, with the main variable being the fraction of Ly α photons able to emerge from the inner few kiloparsec region without being destroyed. For example, the difference between the Ly α Em and Ly α Abs (see Table 2) spectrally classified subsets is an overall factor of ~ 5 in the Ly α surface brightness at the full continuum extent (Figure 6), beyond which the ratio of $S(b)$ for the two sub-samples remains essentially constant. The scale lengths for Ly α emission ($b_l \simeq 25 \pm 3$ kpc) are consistent among the statistically distinct galaxy sub-samples in spite of the fact that the integrated line-to-continuum ratio varies by large factors among the same sub-samples.

5.1. Previous Results on Statistical Ly α Detections

Ly α emission with physical extent larger than that of a galaxy’s continuum starlight is not a surprising result from a theoretical perspective (e.g., Barnes & Haehnelt 2009, 2010; Laursen et al. 2009a, 2009b), and has been observed and noted in many individual cases both in the nearby (e.g., Mas-Hesse et al. 2003; Hayes et al. 2007; Östlin et al. 2009) and high-redshift (e.g., Franx et al. 1997; Möller & Warren 1998; Steidel et al. 2000; Fynbo et al. 2003; Matsuda et al. 2004; Adelberger et al. 2006; Ouchi et al. 2008) universe. However, relatively few surveys at high redshift have reached adequate Ly α surface brightness limits to allow the detection of the very low surface brightness levels discussed above. An exception is the extremely deep spectroscopic survey for Ly α emission conducted by Rauch et al. (2008, hereafter R08). Using an Ly α -selected sample distributed over the redshift range $2.7 \leq z \leq 3.8$, these authors noted that extended Ly α emission was a common feature of the LAEs discovered in their survey. A spatial stack of all of the Ly α emitting sources exhibited significant emission (with threshold $\simeq 1.5 \times 10^{-19}$ erg s $^{-1}$ cm $^{-2}$ arcsec $^{-2}$) to an angular scale of $\sim 4''$, or ~ 30 kpc projected physical radius. The R08 sample, as the authors themselves point out, covers a different range of UV luminosity compared to most continuum-selected LBG spectroscopic surveys—only one of 27 objects has $V < 25.5$, while 80% our sample (which has a median $V \simeq 25.0$) has $V < 25.5$, although there is a tendency for the faintest objects to be among those with the strongest Ly α emission lines (see Tables 2 and 3).²⁷ Nevertheless, the average surface brightness profile for the R08 Ly α -selected sample is remarkably similar to that of our continuum-selected sample (e.g., compare Figure 6 to Figure 20 of R08). For objects in our “Ly α Em” sub-sample (Table 2), the peak Ly α SBs are

²⁶ Note that our procedure of masking out all identified continuum sources other than the central one when producing the Ly α and continuum stacks (Section 3) would suppress what Zheng et al. (2010b) call the “two-halo term” due to clustering, so our observed Ly α profiles should be compared only with the “one-halo,” central component.

²⁷ Moving our continuum-selected sample to the somewhat higher median redshift of R08 would result in $\simeq 50\%$ of our sample having $V > 25.5$.

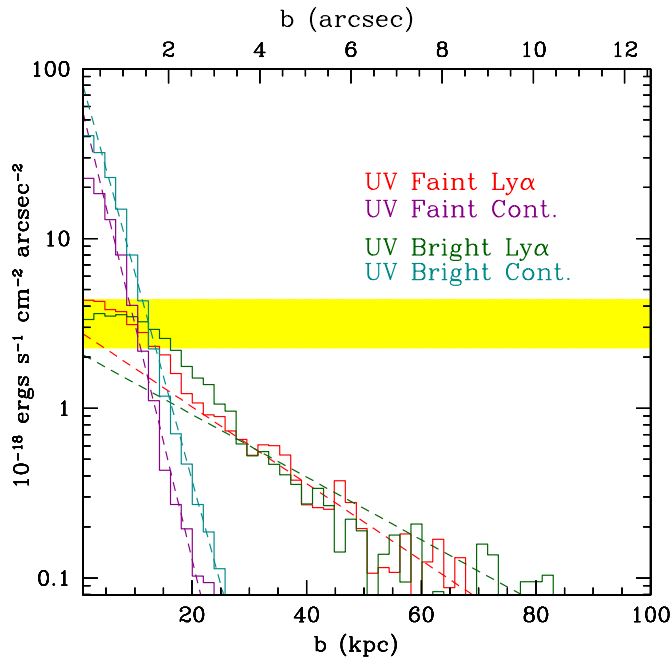


Figure 14. Comparison of the continuum and Ly α surface brightness profiles of the full sample divided into two at the median continuum apparent magnitude. The “UV bright” sample is a factor of $\simeq 2.0$ times brighter in the continuum than that of the “UV faint” sample (CB(bright) = 24.22 vs. CB(faint) = 24.95), but the average Ly α flux for the UV bright sub-sample is 10% smaller than that of the UV-faint sub-sample, i.e., $W_0(\text{Ly}\alpha, \text{bright}) = 22.0 \text{ \AA}$, while $W_0(\text{Ly}\alpha, \text{faint}) = 48.5 \text{ \AA}$.

(A color version of this figure is available in the online journal.)

somewhat higher than for the R08 sample, while the angular extent (at the same limiting SB of $\sim 1 \times 10^{-19} \text{ erg s}^{-1} \text{ cm}^{-2} \text{ arcsec}^{-2}$) is $\simeq 2.5\text{--}3$ times larger in the present LBG sample. Within our sample there is a significant dependence of $W_0(\text{Ly}\alpha)$ on apparent UV continuum luminosity, but the average Ly α profiles are similar, as shown in Figure 14.

In any case, it is worth pointing out that, under the hypothesis that Ly α scattering, and not fluorescence, is the dominant process producing the observed Ly α halos, the scattering medium need not be optically thick in the H I Lyman continuum. This means that it would be incorrect to associate the observed physical extent of Ly α emission with regions having $N(\text{H I}) > 3 \times 10^{18} \text{ cm}^{-2}$ as R08 have suggested—in principle, $N(\text{H I})$ could be 1000 times lower and still remain optically thick to Ly α photons.

Perhaps more directly analogous to the results of the present sample is the NB Ly α survey of Hayashino et al. (2004). These authors used deep NB Ly α images in the SSA22 field, and stacked the Ly α images of 22 $z = 3.09$ continuum-selected LBGs from the survey of Steidel et al. (2003), of which 19 are in common with our current SSA22 sample.²⁸ Indeed, Hayashino et al. showed that significant emission extends to angular scales of at least $4''$, and that the “ring” in the range $2''\text{--}4''$ often contains as much or more Ly α flux than the inner $\theta \leq 2''$ region. They also stated (but did not show) that a stack of the 13 galaxies did not individually exhibit extended Ly α emission results in a significant detection on the same $2''\text{--}4''$ scales. Although the authors did not discuss what physical mechanism might

have been responsible for their observation, these results clearly provided an early indication of the nature of Ly α emission in L^* galaxies, borne out by our larger and more sensitive sample.

5.2. Has the Whole Iceberg Been Detected?

The level of sensitivity to low-SB Ly α emission at high redshifts is unlikely to improve by large factors using the current generation of ground-based telescopes, and so a natural question would be: How much more is there at still lower SB? Many Ly α surveys (e.g., Rauch et al. 2008; Bunker et al. 1998) have been designed to detect Ly α fluorescence induced by the metagalactic radiation field at redshifts $2 \lesssim z \lesssim 3$. The radiation field intensity is usually expressed as $J_\nu \simeq (2\text{--}10) \times 10^{-22} \text{ erg s}^{-1} \text{ cm}^{-2} \text{ Hz}^{-1} \text{ sr}^{-1}$, where the quoted range indicates the dispersion among published observational or theoretical estimates (e.g., Shapley et al. 2006; Bolton et al. 2005; Scott et al. 2000; Faucher-Giguère et al. 2008). The expected maximum fluorescent signal at $z \simeq 2.5\text{--}3.0$ is in the range $(0.2\text{--}2) \times 10^{-19} \text{ erg s}^{-1} \text{ cm}^{-2} \text{ arcsec}^{-2}$ if the only source of ionizing photons is the general UV background (see, e.g., Cantalupo et al. 2005; Kollmeier et al. 2010; Faucher-Giguère et al. 2011). These expectations clearly lie at or below the current SB thresholds of any survey completed to date. The difficulty of detecting the fluorescent signal from the metagalactic UV field has instead inspired several searches for fluorescence near bright sources of ionizing photons, such as QSOs (Francis & Bland-Hawthorn 2004; Cantalupo et al. 2005; Adelberger et al. 2006; Hennawi et al. 2009). The results from such studies have been mixed.

A different argument can be used to suggest that fluorescence from the UV background will always be overwhelmed by Ly α scattering from the CGM of star-forming galaxies, at least at $z \sim 2\text{--}3$. This assertion follows from the fact that S2010 found that the total absorption cross section contributed by the CGM of LBGs (using $R_{\text{eff}} = 80\text{--}90 \text{ kpc}$ for the detection of low-ionization absorption species) can account for a large fraction of all gas with $N(\text{H I}) \gtrsim 2 \times 10^{17} \text{ cm}^{-2}$ (i.e., $\tau \gtrsim 1$ in the Lyman continuum, also known as “Lyman limit systems”). In other words, any gas of sufficiently high $N(\text{H I})$ to produce a detectable signal from fluorescence also lies within $\sim 90 \text{ kpc}$ of a star-forming galaxy with properties similar to those in our sample. We have shown that these galaxies generically exhibit diffuse Ly α emission on the same physical scales when a surface brightness threshold of $S(\text{Ly}\alpha) \sim 1 \times 10^{-19} \text{ erg s}^{-1} \text{ cm}^{-2} \text{ arcsec}^{-2}$ is reached. Unless the fluorescent Ly α signal lies at the very top of the allowed range, it will have much lower SB than the signal we have attributed to scattering from the inside of the galaxy out.

It is more difficult to assess what fraction of observed Ly α emission may be due to cooling processes such as those described by a number of recent authors (e.g., Dijkstra & Loeb 2009; Kollmeier et al. 2010; Faucher-Giguère et al. 2011; Goerdt et al. 2010). In particular, the predictions of the emergent Ly α emission from cooling gas accreting onto galaxies are extremely sensitive to gas temperature (Kollmeier et al. 2010; Faucher-Giguère et al. 2011) and to the small-scale structure in the gas. As a result, the range in Ly α flux and SB, as well as the galaxy mass dependence and spatial distribution of cooling emission, must be regarded as uncertain by a factor of $\gtrsim 10$, with an upper bound (based on energetic arguments) that can be as large as $L(\text{Ly}\alpha) \gtrsim 10^{44} \text{ erg s}^{-1}$, but which under different assumptions could be as small as $\sim 5 \times 10^{41} \text{ erg s}^{-1}$ for a galaxy with $M_{\text{halo}} \simeq 9 \times 10^{11} M_\odot$ (Faucher-Giguère et al. 2011),

²⁸ The new NB image used in the present sample includes both archival Subaru data as well as an additional 10 hr integration using LRIS on the Keck 1 telescope, and so is substantially deeper (\sim factor of 2–3), but covers a much smaller area, than that of Hayashino et al. (2004).

approximately the mean halo mass of the galaxies in the present sample (see Adelberger et al. 2005; Conroy et al. 2008; Steidel et al. 2010).

The observations appear to argue against a significant contribution of cooling radiation to the detected Ly α halos, at least on average. We have shown that the shape of the observed radial surface brightness distribution among the LBGs in the sample is remarkably consistent beyond the inner ~ 10 kpc, within which the Ly α intensity for a given continuum luminosity varies by orders of magnitude. Moreover, the overall intensity scaling for the Ly α emission at large radii is strongly correlated with the behavior of Ly α emission in the inner 5–10 kpc region—at the same continuum luminosity, Ly α absorption-dominated galaxies (on average) exhibit diffuse Ly α emission with a factor of 3–4 lower normalization than galaxies with spectroscopically detected Ly α emission. In the context of Ly α cooling radiation, one might expect the extended Ly α emission to be strongly correlated with galaxy mass and/or SFR since it is believed by some (e.g., Goerdt et al. 2010) that the baryonic accretion rate ultimately controls the SFR. In this scenario, the central region of Ly α emission might be suppressed by higher H I column densities mixed with dust, but the outer regions would have no obvious way to “know about” the number of Ly α photons being produced at smaller radii. Instead, one might expect that the brightest Ly α halos would be associated with the “Ly α Abs” sub-sample, since these have a median SFR nearly 3 (4.5) times larger than the “Ly α Em” (LAE) sub-samples. Clearly, the observations are inconsistent with this expectation. If on the other hand most or all of the Ly α emission at all radii originates in the central regions and is subsequently scattered by the CGM gas, the density of photons available for scattering at (for example) $r = 50$ kpc will be very tightly linked to the number of Ly α photons that successfully diffuse past $r \sim 5$ kpc, beyond which the Ly α halos appear “self-similar.” The emergent Ly α luminosities are entirely consistent with the observed level of star formation in the galaxies, and are more attenuated than the UV continuum, for all sub-samples except the LAEs. It is not necessary to invoke sources of Ly α emission other than scattering (from the inside outward) to account for both the Ly α luminosity and its spatial distribution.

Under the scattering hypothesis, and further assuming that the scattering medium is self-similar for all galaxies, then sub-samples with more luminous Ly α halos should provide information on the degree to which even the current SB threshold might lead to an underestimate of the total Ly α flux emergent from a galaxy. To increase the dynamic range for detecting diffuse Ly α emission, one might use the observed properties of giant LABs (which are well-detected in the stack to $b \simeq 15''$) to estimate how much additional Ly α flux may lie beyond the SB detection threshold near $b \sim 8''$ for more typical galaxies. Under the assumption that diffuse emission from LABs and LBGs has a similar origin and differs only in total Ly α luminosity, the curve of growth for LABs (Figure 10) suggests that an aperture of radius $\simeq 8''$ would underestimate the total Ly α flux by only $\sim 10\%$. Thus, further aperture corrections to the integrated Ly α would probably leave the values of $W_0(\text{Ly}\alpha)$ (Table 2) and $f_{\text{esc,rel}}(\text{Ly}\alpha)$ (Table 3) more or less unchanged. At least at $z \simeq 2.65$, the current SB limit appears to be sufficient to detect most of the “iceberg.”

Finally, we note that the differences in the intensity of the large-scale diffuse emission among sub-samples divided according to their spectral morphology suggest that galaxy viewing angle is relatively unimportant (on average) for Ly α

emission; that is, most galaxies are not LAEs in some directions but strong Ly α Abs systems in others, consistent with the inference of generally axisymmetric CGM gas distributions inferred from the absorption line studies (S2010).

5.3. IS Absorption, Ly α Emission, and the CGM

Perhaps the strongest correlation (first explored in detail by Shapley et al. 2003 for galaxies at $z \sim 3$) among the observed spectral properties of LBGs is between the strength of low-ionization IS absorption lines and the spectral morphology and equivalent width of Ly α . Galaxies with the strongest Ly α emission (among the continuum-selected samples) invariably have much *weaker* than average low-ionization IS absorption lines (see Erb et al. 2010 for a well-observed example), while those with the Ly α appearing strongly in absorption have correspondingly strong IS absorption features, often reaching zero intensity over some or most of the line profile (see, e.g., Pettini et al. 2002), indicating unity covering fraction. These trends are easy to understand in the context of the CGM model discussed by S2010 and extended in this paper to cover the expectations for Ly α scattering and its effects on the observability of Ly α emission: both the IS absorption lines and Ly α line strengths and morphologies are controlled by the kinematics and geometry of the same IS and circumgalactic gas.

Dust certainly plays a role in determining the fraction of both Ly α and continuum photons that will end up reaching an observer. However, the gas-phase geometry and kinematics are more directly responsible for the observed line strength (and line-to-continuum ratios) in the spectra. If a galaxy has strong Ly α emission emerging from the same region as the UV continuum, it *must* have shallow IS absorption lines; if it did not, then at least the spatial distribution of Ly α (if not also its integrated flux) would be substantially modified—it would become more spatially diffuse. When a slit spectrum (generally a small-aperture measurement) shows very strong and deep low-ionization IS absorption lines, including Ly α , it *must* be the case that any Ly α seen in emission will have escaped either from a region spatially distinct from the continuum (the subject of this paper), or by way of scattering from very high velocity material (see S2010). Ly α emission seen in spectra which also show strong IS absorption will be primarily in the latter category, hence the nearly universal systemic redshift of Ly α emission in LBG spectra. We have emphasized above that any Ly α photons that are not destroyed by dust will eventually find their way out of their host galaxy—but will be much harder to detect by the time they do.

The point is that IS absorption and Ly α emission are causally intertwined through their mutual dependence on the structure and kinematics of the CGM on scales from a few kpc to $\simeq 100$ kpc.

6. SUMMARY

We have presented observations of a sample of 92 continuum-selected LBGs at $\langle z \rangle = 2.65$ having both rest-UV spectra and very deep NB Ly α images. The sample, which is representative of $\simeq L^*$ LBGs at $2 \lesssim z \lesssim 3$, was used to examine the nature of diffuse Ly α emission from star-forming galaxies as function of their spectral morphologies and NB-inferred Ly α fluxes. By stacking both UV continuum and Ly α line images for subsets of the galaxy sample, we are able to study the spatial distribution of Ly α and continuum emission to much

lower surface brightness thresholds ($\sim 1 \times 10^{-19}$ erg s $^{-1}$ cm $^{-2}$ arcsec $^{-2}$) than would be possible for individual galaxies. We find the following.

1. Relatively luminous star-forming galaxies generically exhibit low surface brightness Ly α emission to projected radii of at least 80 physical kpc (~ 10 arcsec). The extended emission is present even for the stacks of LBGs that would be classified based on their spectra as having Ly α in net absorption. The Ly α line to UV continuum ratio is always strongly suppressed in the central regions of galaxies relative to “Case B” expectations, but beyond galactocentric radii of $r \simeq 5$ kpc, where the continuum light falls off very rapidly, Ly α emission begins to dominate.
2. The Ly α emitting regions have characteristic exponential scale lengths 5–10 times larger than the corresponding UV continuum emission *from the same galaxies*. It appears that on average *all* classes of star-forming galaxies in the observed range of luminosity would be classified as LABs if the observations were sufficiently sensitive. Similarly, nearly all galaxies would also be classified as LAEs if their total Ly α flux were measured using a sufficiently large aperture. Spectroscopic measurements (or, typically deep Ly α NB surveys) of Ly α emission underestimate the total Ly α flux (or, equivalently, the rest equivalent width $W_0(\text{Ly}\alpha)$) by an average factor of 5, and a factor of >3 even for those classified as LAEs.
3. The surface brightness distribution, total flux, and scale lengths for Ly α emission are all consistent with a picture in which most or all detectable Ly α emission is produced in H II regions spatially coincident with the galaxies’ UV continuum emission. The Ly α surface brightness is then modified by scattering from the surface of H I clouds that are being driven to large galactocentric radii by galaxy-scale outflows. The spatial extent of observed Ly α emission is then dictated by the spatial extent of circum-galactic gas with sufficiently large covering fraction to have a finite chance of scattering Ly α photons in the direction of an observer.
4. The inferred attenuation of Ly α emission from continuum-selected LBGs is consistently larger than that of the UV continuum ($A(\text{Ly}\alpha) \simeq 1.6A(\text{UV})$) for all sub-samples except LAEs, which have $A(\text{Ly}\alpha) \simeq A(\text{UV})$. Most of the attenuation of Ly α emission appears to occur within ~ 5 kpc of the continuum centroid of a galaxy. While the fraction of a galaxies’ total Ly α photon production that is able to diffuse beyond ~ 5 kpc varies substantially, the scattering halo of cool material at larger radii leads to self-similar diffuse Ly α halos. A simple scattering model for Ly α emission was presented, based on the structure of the CGM gas inferred from measurements of absorption in lines of sight passing within $b < 125$ kpc of an ensemble of similar galaxies. The model successfully accounts for both the typical size and the surface brightness profile of Ly α emission.
5. We argue that scattering of Ly α photons from circum-galactic gas can account for all of the observations of continuum-selected star-forming galaxies, and that the observed correlations of the intensity of diffuse Ly α halos with the spectral morphology of the central galaxies argues against a significant contribution from Ly α cooling of accreting gas. We also argue that Ly α scattering processes will always dominate over fluorescence (caused either by the metagalactic ionizing radiation field or by ionizing

photons from inside the galaxy) in producing spatially extended Ly α emission.

6. Ly α emission and IS absorption line strengths are causally intertwined through their mutual dependence on the structure and kinematics of CGM gas. Galaxies with strong and centrally peaked Ly α emission are expected to be associated with shallow IS absorption lines, while strong Ly α absorption lines that completely absorb the UV continuum light of the host galaxy force Ly α emission to larger galactocentric radii before escaping the host galaxy.

The detection of diffuse Ly α emission halos at the current surface brightness level has required the equivalent of $\simeq 200$ – 1000 hr integration time with a 10 m class telescope (accounting for the effective integration time of the stacked Ly α line images). Given the $(1+z)^{-4}$ dependence of observed Ly α surface brightness (for a given physical luminosity surface density), it is not feasible at present to obtain similar results at significantly higher redshifts. However, vastly increasing the number of continuum-selected LBGs with sensitive NB Ly α observations could in principle trace Ly α emission from galaxy halos until they become indistinguishable from the background. Together with observations of the cool gas phase via absorption lines in the spectra of background sources (both galaxies and QSOs), such Ly α emission observations considerably enhance our ability to observe directly the distribution of cool baryons and their flow rate into and out of forming galaxies during an undoubtedly crucial (but not well-understood) period in cosmic history.

This work has been supported by the US National Science Foundation through grants AST-0606912 and AST-0908805 (C.C.S.), and by the David and Lucile Packard Foundation (A.E.S.). C.C.S. acknowledges additional support from the John D. and Catherine T. MacArthur Foundation and the Peter and Patricia Gruber Foundation. D.K.E. was supported by the National Aeronautics and Space Administration under Award No. NAS7-03001 and the California Institute of Technology. Gwen Rudie and Olivera Rakic each provided very helpful comments on an earlier draft of the paper; we also thank Kurt Adelberger for his early involvement in the work which made the new results possible. We are grateful to the staff of the W. M. Keck Observatory who keep the instruments and telescopes running effectively. A careful reading and constructive report by the referee is very much appreciated. Finally, we wish to extend thanks to those of Hawaiian ancestry on whose sacred mountain we are privileged to be guests.

REFERENCES

- Adelberger, K. L., & Steidel, C. C. 2000, *ApJ*, **544**, 218
 Adelberger, K. L., Steidel, C. C., Kollmeier, J. A., & Reddy, N. A. 2006, *ApJ*, **637**, 74
 Adelberger, K. L., Steidel, C. C., Pettini, M., Shapley, A. E., Reddy, N. A., & Erb, D. K. 2005, *ApJ*, **619**, 697
 Adelberger, K. L., Steidel, C. C., Shapley, A. E., Hunt, M. P., Erb, D. K., Reddy, N. A., & Pettini, M. 2004, *ApJ*, **607**, 226
 Barnes, L. A., & Haehnelt, M. G. 2009, *MNRAS*, **397**, 511
 Barnes, L. A., & Haehnelt, M. G. 2010, *MNRAS*, **403**, 870
 Barnes, L. A., Haehnelt, M. G., Tescari, E., & Viel, M. 2011, arXiv:1101.3319
 Bertin, E., & Arnouts, S. 1996, *A&AS*, **117**, 393
 Bolton, J. S., Haehnelt, M. G., Viel, M., & Springel, V. 2005, *MNRAS*, **357**, 1178
 Brocklehurst, M. 1971, *MNRAS*, **153**, 471
 Bunker, A. J., Marleau, F. R., & Graham, J. R. 1998, *AJ*, **116**, 2086

- Calzetti, D., Armus, L., Bohlin, R. C., Kinney, A. L., Koornneef, J., & Storchi-Bergmann, T. 2000, *ApJ*, **533**, 682
- Cantalupo, S., Porciani, C., Lilly, S. J., & Miniati, F. 2005, *ApJ*, **628**, 61
- Chabrier, G. 2003, *PASP*, **115**, 763
- Charlot, S., & Fall, S. M. 1993, *ApJ*, **415**, 580
- Conroy, C., Shapley, A. E., Tinker, J. L., Santos, M. R., & Lemson, G. 2008, *ApJ*, **679**, 1192
- Dijkstra, M., Haiman, Z., & Spaans, M. 2006, *ApJ*, **649**, 37
- Dijkstra, M., & Loeb, A. 2009, *MNRAS*, **400**, 1109
- Erb, D. K., Pettini, M., Shapley, A. E., Steidel, C. C., Law, D. R., & Reddy, N. A. 2010, *ApJ*, **719**, 1168
- Erb, D. K., Steidel, C. C., Shapley, A. E., Pettini, M., Reddy, N. A., & Adelberger, K. L. 2006a, *ApJ*, **647**, 128
- Erb, D. K., Steidel, C. C., Shapley, A. E., Pettini, M., Reddy, N. A., & Adelberger, K. L. 2006b, *ApJ*, **646**, 107
- Faucher-Giguere, C., Keres, D., Dijkstra, M., Hernquist, L., & Zaldarriaga, M. 2011, *MNRAS*, in press (arXiv:1011.1693)
- Faucher-Giguere, C., Lidz, A., Hernquist, L., & Zaldarriaga, M. 2008, *ApJ*, **682**, L9
- Finkelstein, S. L., Rhoads, J. E., Malhotra, S., Grogan, N., & Wang, J. 2008, *ApJ*, **678**, 655
- Förster Schreiber, N. M., et al. 2009, *ApJ*, **706**, 1364
- Francis, P. J., & Bland-Hawthorn, J. 2004, *MNRAS*, **353**, 301
- Franx, M., Illingworth, G. D., Kelson, D. D., van Dokkum, P. G., & Tran, K.-V. 1997, *ApJ*, **486**, L75
- Fynbo, J. P. U., Ledoux, C., Möller, P., Thomsen, B., & Burud, I. 2003, *A&A*, **407**, 147
- Goerdt, T., Dekel, A., Sternberg, A., Ceverino, D., Teyssier, R., & Primack, J. R. 2010, *MNRAS*, **407**, 613
- Gronwall, C., et al. 2007, *ApJ*, **667**, 79
- Hartmann, L. W., Huchra, J. P., & Geller, M. J. 1984, *ApJ*, **287**, 487
- Hayashino, T., et al. 2004, *AJ*, **128**, 2073
- Hayes, M., Östlin, G., Atek, H., Kunth, D., Mas-Hesse, J. M., Leitherer, C., Jiménez-Bailón, E., & Adamo, A. 2007, *MNRAS*, **382**, 1465
- Hayes, M., et al. 2010, *Nature*, **464**, 562
- Hennawi, J. F., Prochaska, J. X., Kollmeier, J., & Zheng, Z. 2009, *ApJ*, **693**, L49
- Kereš, D., Katz, N., Davé, R., Fardal, M., & Weinberg, D. H. 2009, *MNRAS*, **396**, 2332
- Kollmeier, J. A., Zheng, Z., Davé, R., Gould, A., Katz, N., Miralda-Escudé, J., & Weinberg, D. H. 2010, *ApJ*, **708**, 1048
- Kornei, K. A., Shapley, A. E., Erb, D. K., Steidel, C. C., Reddy, N. A., Pettini, M., & Bogosavljević, M. 2010, *ApJ*, **711**, 693
- Laursen, P., Razoumov, A. O., & Sommer-Larsen, J. 2009a, *ApJ*, **696**, 853
- Laursen, P., Sommer-Larsen, J., & Andersen, A. C. 2009b, *ApJ*, **704**, 1640
- Law, D. R., Steidel, C. C., Erb, D. K., Pettini, M., Reddy, N. A., Shapley, A. E., Adelberger, K. L., & Simenc, D. J. 2007, *ApJ*, **656**, 1
- Leitherer, C., et al. 1999, *ApJS*, **123**, 3
- Madau, P., Pozzetti, L., & Dickinson, M. 1998, *ApJ*, **498**, 106
- Mas-Hesse, J. M., Kunth, D., Tenorio-Tagle, G., Leitherer, C., Terlevich, R. J., & Terlevich, E. 2003, *ApJ*, **598**, 858
- Matsuda, Y., et al. 2004, *AJ*, **128**, 569
- Meier, D. L. 1976, *ApJ*, **207**, 343
- Meier, D. L., & Terlevich, R. 1981, *ApJ*, **246**, L109
- Meurer, G. R., Heckman, T. M., & Calzetti, D. 1999, *ApJ*, **521**, 64
- Moller, P., & Warren, S. J. 1998, *MNRAS*, **299**, 661
- Nestor, D. B., Shapley, A. E., Steidel, C. C., & Siana, B. 2011, *ApJ*, in press (arXiv:1102.0286)
- Neufeld, D. A. 1990, *ApJ*, **350**, 216
- Neufeld, D. A. 1991, *ApJ*, **370**, L85
- Nilsson, K. K., Tapken, C., Möller, P., Freudling, W., Fynbo, J. P. U., Meisenheimer, K., Laursen, P., & Östlin, G. 2009, *A&A*, **498**, 13
- Oke, J. B., et al. 1995, *PASP*, **107**, 375
- Östlin, G., Hayes, M., Kunth, D., Mas-Hesse, J. M., Leitherer, C., Petrosian, A., & Atek, H. 2009, *AJ*, **138**, 923
- Ouchi, M., et al. 2008, *ApJS*, **176**, 301
- Partridge, R. B., & Peebles, P. J. E. 1967, *ApJ*, **147**, 868
- Peter, A. H. G., Shapley, A. E., Law, D. R., Steidel, C. C., Erb, D. K., Reddy, N. A., & Pettini, M. 2007, *ApJ*, **668**, 23
- Pettini, M., Rix, S. A., Steidel, C. C., Adelberger, K. L., Hunt, M. P., & Shapley, A. E. 2002, *ApJ*, **569**, 742
- Pettini, M., Steidel, C. C., Adelberger, K. L., Dickinson, M., & Giavalisco, M. 2000, *ApJ*, **528**, 96
- Rauch, M., et al. 2008, *ApJ*, **681**, 856
- Reddy, N. A., Erb, D. K., Pettini, M., Steidel, C. C., & Shapley, A. E. 2010, *ApJ*, **712**, 1070
- Reddy, N. A., & Steidel, C. C. 2009, *ApJ*, **692**, 778
- Reddy, N. A., Steidel, C. C., Fadda, D., Yan, L., Pettini, M., Shapley, A. E., Erb, D. K., & Adelberger, K. L. 2006, *ApJ*, **644**, 792
- Reddy, N. A., Steidel, C. C., Pettini, M., Adelberger, K. L., Shapley, A. E., Erb, D. K., & Dickinson, M. 2008, *ApJS*, **175**, 48
- Salpeter, E. E. 1955, *ApJ*, **121**, 161
- Scott, J., Bechtold, J., Dobrzycki, A., & Kulkarni, V. P. 2000, *ApJS*, **130**, 67
- Shapley, A. E., Steidel, C. C., Erb, D. K., Reddy, N. A., Adelberger, K. L., Pettini, M., Barmby, P., & Huang, J. 2005, *ApJ*, **626**, 698
- Shapley, A. E., Steidel, C. C., Pettini, M., & Adelberger, K. L. 2003, *ApJ*, **588**, 65
- Shapley, A. E., Steidel, C. C., Pettini, M., Adelberger, K. L., & Erb, D. K. 2006, *ApJ*, **651**, 688
- Spitzer, L. 1978, *Physical Processes in the Interstellar Medium* (New York: Wiley-Interscience)
- Steidel, C. C., Adelberger, K. L., Dickinson, M., Giavalisco, M., Pettini, M., & Kellogg, M. 1998, *ApJ*, **492**, 428
- Steidel, C. C., Adelberger, K. L., Giavalisco, M., Dickinson, M., & Pettini, M. 1999, *ApJ*, **519**, 1
- Steidel, C. C., Adelberger, K. L., Shapley, A. E., Erb, D. K., Reddy, N. A., & Pettini, M. 2005, *ApJ*, **626**, 44
- Steidel, C. C., Adelberger, K. L., Shapley, A. E., Pettini, M., Dickinson, M., & Giavalisco, M. 2000, *ApJ*, **532**, 170
- Steidel, C. C., Adelberger, K. L., Shapley, A. E., Pettini, M., Dickinson, M., & Giavalisco, M. 2003, *ApJ*, **592**, 728
- Steidel, C. C., Erb, D. K., Shapley, A. E., Pettini, M., Reddy, N. A., Bogosavljević, M., Rudie, G. C., & Rakic, O. 2010, *ApJ*, **717**, 289
- Steidel, C. C., Shapley, A. E., Pettini, M., Adelberger, K. L., Erb, D. K., Reddy, N. A., & Hunt, M. P. 2004, *ApJ*, **604**, 534
- Verhamme, A., Schaerer, D., Atek, H., & Tapken, C. 2008, *A&A*, **491**, 89
- Zheng, Z., Cen, R., Trac, H., & Miralda-Escudé, J. 2010a, *ApJ*, **716**, 574
- Zheng, Z., Cen, R., Weinberg, D., Trac, H., & Miralda-Escudé, J. 2010b, arXiv:1010.3017